Article

Not peer-reviewed version

Optimal Branch Bending Angle for Korla Fragrant Pear: A Multi-Trait Physiological Trade-Off Framework

Ablah Niyaz , Mansur Nasir * , Shikui Zhang , Peng Wangshao , Min Cuihui , Guoquan Fan , Dilraba Muhtar , Xianbiao Ma , Mirigul Tunyaz , Lihong Yao , Ruizhe Wang , Tianming He , Juan Song , Mayira Eziz

Posted Date: 25 December 2025

doi: 10.20944/preprints202512.2343.v1

Keywords: *Pyrus sinkiangensis*; branch bending angle; carbon–hormone synergy; fruit set; canopy management; high-density orchard

Article

Optimal Branch Bending Angle for Korla Fragrant Pear: A Multi-Trait Physiological Trade-Off Framework

Ablah Niyaz [1,†], Mansur Nasir [2,*,†], Shikui Zhang [3], Peng Wangshao [3], Min Cuihui [2], Guoquan Fan [4], Dilraba Muhtar [2], Xianbiao Ma [2], Mirigul Tunyaz [2], Lihong Yao [2], Ruizhe Wang [2], Tianming He [2], Juan Song [5] and Mayira Eziz [5]

[1] Turpan Experimental Station, Xinjiang Academy of Agricultural Sciences, Uygur Autonomous Region, Turpan 838000, Xinjiang, China
[2] College of Horticulture, Xinjiang Agricultural University, Urumqi 830052, China
[3] Institute of Horticultural Crops, Xinjiang Academy of Agricultural Sciences (National Fruit Tree Germplasm Resources Luntai Fruit Tree Resource Garden), Luntai 841600, Xinjiang, China
[4] Department of Agricultural Science and Technology Achievement Transformation, Xinjiang Academy of Agricultural Sciences, Urumqi 830000, Xinjiang, China
[5] Institute of Forestry and Horticulture, Aksu Agricultural Science and Technology Innovation Center, Aksu 843000, Xinjiang, China
* Correspondence: mansurnasir@163.com or mansur813@163.com; Tel: +86-133-7977-0813
† These authors contributed equally as first authors.

Highlights

- First physiology-based optimization of the branch angle of Korla fragrant pear
- 80° pulling maximizes the fruit set (11.8%) via synergy between sugars and hormones
- The GA_4/GA_7 surge on 28 April triggers calyx abscission and ovary growth
- PCA of 57 traits reveals 80° as the system-wide optimum (D=0.718)
- These findings provide nonchemical management targets for arid-region pear orchards

Abstract

The optimal branch bending angle for *Pyrus sinkiangensis* Yü (Korla fragrant pear) remains undefined. In this study, the optimal angle was determined by integrating the phenological, nutritional, hormonal, and fruit-quality responses across a 15-day bloom window. Four branch angles (40°, 60°, 80°, and 100°) were applied to 8-year-old trees in spring 2022, and flowering dynamics, bud carbon/nitrogen status, leaf morphology/mineral content, fruiting-shoot architecture, endogenous hormones, and fruit quality were comprehensively evaluated. The 80° angle maximized the fruit set (11.77%) and bud soluble sugar content (8.84 mg/g DW), significantly outperforming the other angles ($p < 0.05$). The flowering rate peaked at 100° (7.89%) but was statistically comparable to that at 60° and 80° ($p > 0.05$); calyx removal was greatest at 60° (73.33%), with no significant difference from that at 80° (71%, $p > 0.05$). These reproductive benefits aligned with enhanced leaf source capacity—80° pulling resulted in the greatest leaf area (59.51 cm^2), the greatest amount of chlorophyll (3.11 mg/g DW), and elevated N/Mg/Cu concentrations. Branch architecture was optimized at 80°, with the percentage of medium fruiting spurs reaching 41.1% and the xylem:phloem dry-weight ratio peaking at 1.78, indicating the development of efficient assimilate transport pathways. Hormonally, 80° triggered a distinct cascade: a transient GA_4/GA_7 surge (50.6 and 1.34 ng/g DW) on 28 April, followed by sustained IAA elevation (2.05 ng/g DW) and zeatin stabilization (0.27–0.29 ng/g DW) during ovary development. Consequently, the fruit quality was comprehensively improved at 80°—the single-fruit weight (110.7 g), soluble sugar content (10.08 mg/g DW), and sugar/acid ratio (17.08) were greatest, whereas the stone-cell content was lowest (0.49 mg/g DW). Principal component analysis of 57 traits confirmed 80° as the system-wide

 doi:10.20944/preprints202512.2343.v1

optimum (D = 0.718). These results demonstrate that an 80° bending angle synchronizes carbohydrate supply, hormone signaling, and fruit quality in Korla fragrant pear, providing a low-cost, nonchemical benchmark for precision canopy management in high-density orchards. **One-sentence summary:** An 80° branch-bending angle optimizes carbon-hormone synergy via a transient GA_4/GA_7 surge and sustained IAA-zeatin signaling, maximizing fruit set and quality in high-density Korla fragrant pear orchards.

Keywords: *Pyrus sinkiangensis*; branch bending angle**;** carbon–hormone synergy; fruit set; canopy management; high-density orchard

Introduction

Branch bending is a foundational horticultural practice that regulates tree architecture, modulates source–sink relationships, and optimizes reproductive success in fruit crops [1,2]. By altering branch orientation, this technique influences light interception, auxin transport, carbohydrate partitioning, and the microclimate at the organ level, ultimately affecting flowering intensity, fruit set, and yield stability [3–6]. In high-density orchard systems—which are now globally adopted for sustainable intensification—precise canopy management is critical for balancing vegetative vigor with reproductive capacity [4]. While the practice has been successfully applied in rosaceous species such as apple (*Malus domestica*) and European pear (*Pyrus communis*) [4,7–10], optimal bending angles remain species- and genotype specific, and their mechanistic underpinnings are largely unexplored in arid-adapted pear cultivars.

Korla fragrant pear (*Pyrus sinkiangensis* Yü) is the cornerstone of Xinjiang's fruit industry; this fruit is cultivated across approximately 64,467 hectares and is prized for its unique aroma, crisp texture, and thin russet-free skin [11]. However, high-density plantings (4 × 2 m spacing) frequently suffer from critically low fruit set, persistent calyx end persistence, suboptimal sugar accumulation, high stone cell content, and a high incidence of coarse-skinned fruit—bottlenecks that diminish marketability and profitability [5,12]. Existing recommendations for branch angles (60–90°) derive largely from empirical observations in temperate-zone cultivars, lacking a physiology-based framework tailored to arid, high-radiation environments [5]. This leaves a critical gap between canopy manipulation and the carbon–hormone–hydraulics nexus that governs reproductive outcomes.

Recent studies have made significant progress in determining optimal bending angles for different fruit tree species. Marked cultivar-specific differences exist in apple: 90° for 'Gala' versus 110° for 'Fuji' to maximize the C/N ratio and alleviate biennial bearing [7,8]. In walnut (*Juglans regia* 'Qianhe 7'), 90° bending increased female flower number by 206.6% and fruit set by 14.1% [3]. For peach (*Prunus persica* 'Luhong 618'), an 85° Y-shaped angle improved light penetration and fruit weight [4]. Wax apple (*Syzygium samarangense*) performs optimally at 65–85° [9,10]. Critically, bending 'Fuji Mishima' at 15 days after full bloom resulted in peak flower bud density, whereas earlier application induced ethylene inhibition [8]. Physiologically, branch bending suppresses polar auxin transport while increasing cytokinin accumulation in buds and upregulating the expression of floral identity genes such as *WUS* [6]. Branch bending significantly affects the metabolic allocation of sorbitol (the primary carbohydrate) and chlorogenic acid (the primary phenolic compound) in pear tissues, with genotype-, organ-, and time-specific responses [13–15]. Hormone regulation involves branch bending, which suppresses vegetative growth and promotes flowering by reducing IAA and GA while increasing ABA and ZR concentrations; however, studies in apple plants further reveal that cultivar-specific maintenance of an optimal (IAA+GA+ZR)/ABA ratio is the key physiological basis for why 'Fuji' requires stronger bending (110°) than 'Gala' does (90°) [7]. Molecularly, the LAZY gene family mediates gravity perception via amyloplast sedimentation, and the PIN3 protein orchestrates asymmetric hormone distribution—a pathway conserved across land plants [6]. Apical control theory further explains how bending breaks assimilate suppression of lower branches, although reaction

 doi:10.20944/preprints202512.2343.v1

wood formation necessitates continuous angle maintenance [16]. However, despite these advances in temperate-zone cultivars, a physiology-based framework remains lacking for arid-adapted pears such as Korla fragrant pear (*Pyrus sinkiangensis* Yü), particularly for systematic analyses of the carbon–hormone–hydraulics nexus. Crucially, no study has integrated temporally resolved hormone dynamics with static morphological, nutritional, and architectural traits to define a system-level optimum for this economically vital cultivar.

To address this gap, we conducted the first comprehensive, multitrait evaluation of four branch angles (40°, 60°, 80°, and 100°) in an 8-year-old orchard, integrating 57 phenotypic, nutritional, and hormonal traits measured across critical developmental stages—from flowering through fruit set to harvest. This framework captures the carbon–hormone–hydraulics nexus, with a 15-day hormone monitoring window during blooms. We hypothesized that branch angle mediates carbon assimilation, nutrient allocation, and hormone dynamics, creating angle-specific trade-offs between reproductive physiology and vegetative stress. Using LC–MS/MS-based hormone profiling, principal component analysis (PCA), and a novel multitrait physiological trade-off framework, we quantified angle-specific effects on reproductive development, identified key trait covariances, and developed a predictive framework for precision canopy management. This work provides a mechanistic template for the transformation of empirical horticultural practices into predictive science, with direct implications for the sustainable intensification of rosaceous fruit crops in water-limited environments.

Materials and Methods

Plant Material and Experimental Site

The trial was conducted at the Luntai Fruit Tree Resource Nursery (41.8° N, 84.1° E, 962 m a.s.l.), Bayingolin, Xinjiang, China. Eight-year-old 'Korla fragrant pear' (*Pyrus sinkiangensis* Yü) trees grafted onto *Dangshansuli* rootstock with 'Zhongai 1' interstock (4 × 2 m spacing) were used. The region has a temperate continental arid climate (annual mean 10.6 °C, 52 mm of precipitation, and 188 frost-free days). Twelve uniform trees were selected and arranged in a randomized complete block design with three replicates per treatment (n = 3 trees). Four branch bending angle treatments (40°, 60°, 80°, and 100° from the vertical) were applied to the main scaffold branches using nylon ties and wooden stakes to fix the branches in early June 2021. Early June was selected as the branch-fixing period to allow a complete annual cycle of carbohydrate accumulation and vascular remodeling, thereby capturing the lagged effects on reproductive physiology in the following spring, as suggested by the time-specific responses reported in previous studies [13–15].

Flowering Phenology and Fruit Set

Flowering stages (initial, full, and petal-fall) were recorded daily. Flowering rate (%) = flower buds/total buds × 100. After the plants were manually thinned to a uniform flower load, the following formula was used: Fruit set rate (%) = (fruits remaining 10 d after the first physiological drop/thinning flowers) × 100. The calyx removal rate (%) = calyx-shed fruits/total fruits × 100 was scored at the end of the second physiological drop.

Bud Nutrients

At the green-cluster stage, terminal buds of short shoots and axillary buds of long shoots were collected, immediately frozen in liquid N_2, freeze-dried, and stored at –80 °C. Soluble sugars were determined by the anthrone-sulfuric colorimetric method, and total nitrogen was measured by the standard Kjeldahl acid-digestion method [7]. Each treatment had five independent replicates.

 doi:10.20944/preprints202512.2343.v1

Leaf Morphology, Chlorophyll and Mineral Elements

In September 2022, 100 healthy leaves per treatment were sampled. The leaf length, width, fresh and dry weights, and area (LI-3100C) were recorded. Chlorophyll a, b and total were extracted in 80% acetone and quantified spectrophotometrically; SPAD values were obtained with a SPAD-502 meter. Minerals (N, Ca, Mg, Fe, Zn, and Cu) were determined by ICP–OES after HNO_3–$HClO_4$ digestion following the methods of Masson et al. [17] with modifications.

Branch Growth and Water Status

After shoot cessation, 20 branches per treatment were classified into short (<5 cm), medium (5–15 cm) and long (>15 cm) fruiting spurs; length and basal diameter were recorded. Five one-year-old branches per treatment were segmented into xylem and phloem; fresh and dry weights were used to calculate the water content (%). The total nitrogen in the xylem and phloem tissues was determined by the Kjeldahl method [18].

Fruit Quality Assessment

At harvest, 30 fruits per treatment were randomly collected. External indices (single-fruit weight, shape index, pedicel length and diameter, surface finish, color and russeting index) and internal indices (flesh firmness, soluble solids, soluble sugar, titratable acidity, vitamin C and stone-cell content) were determined as described previously [12].

Endogenous Hormone Profiling During the Young-Fruit Stage

Young fruits were sampled every 3 days from 19 April (the second day after full bloom in the 40° and 60° plots and the third day in the 80° and 100° plots) until 4 May (when calyx abscission was >95%). Ten fruits per replicate were pooled, immediately frozen in liquid N_2 and stored at –80 °C. Endogenous hormones (IAA, ABA, GA_1, GA_3, GA_4, GA_7, SA, JA, cis-zeatin, and trans-zeatin) were extracted and purified by a modified method [19] and analyzed by LC–MS/MS (Shimadzu LC-30AD coupled with AB Sciex QTRAP 6500+).

Statistical Analysis

All the data were analyzed in SPSS 27.0. One-way ANOVA followed by Duncan's test was applied when $P < 0.05$. Correlation heatmaps and radar charts were generated with OriginPro 2025 (OriginLab Corporation, USA).

Principal component analysis (PCA) and comprehensive evaluation

To integrate the 57 phenotypic and physiological traits into a single ranking metric, PCA was performed. Three principal components (PC1–PC3) were extracted and rotated using the varimax method. The component scores were transformed into comprehensive indices (CI_1, CI_2, CI_3) and combined into a final evaluation score (D) using the membership function approach. Higher D values indicate superior overall performance. All PCA computations were carried out in OriginPro 2025.

2. Results

To systematically evaluate how the branch-bending angle regulates reproductive development and whole-plant physiology in *Pyrus sinkiangensis*, we quantified (i) flowering phenology, (ii) flowering rate, fruit set and calyx removal, (iii) bud soluble sugar and nitrogen, (iv) leaf fresh/dry mass, area and chlorophyll, (v) leaf mineral profile, (vi) fruiting-shoot typology and dimensions, (vii) xylem vs. phloem water content, (viii) branch nitrogen and dry-mass partitioning, (ix) external and internal fruit quality, (x) young-fruit endogenous hormone dynamics, and (xi) trait intercorrelations via heat-map and radar analyses. The resulting datasets were integrated by univariate statistics and

 doi:10.20944/preprints202512.2343.v1

principal component analysis to identify the canopy configuration best suited for high-density pear orchards.

2.1. Impact of Branch Bending Angle on the Flowering Phenology of Korla Fragrant Pear

We first tested whether the bending angle shifts the timing of key flowering events. Regardless of treatment, bud burst occurred uniformly on 5 April, while full bloom peaked on 14–15 April, and petal fall was completed by 24–26 April, resulting in an overall flowering window of ca. 11 days (Figure 1). Only marginal angle effects were detected: initial flowering was delayed by 1 day under 80° and 100° relative to 40° and 60°, and the blossom-drop phase of 100° lasted one day longer than that of 80° ($P < 0.05$). Thus, larger bending angles slightly delayed anthesis and extended the blooming period without advancing or shortening the entire flowering season.

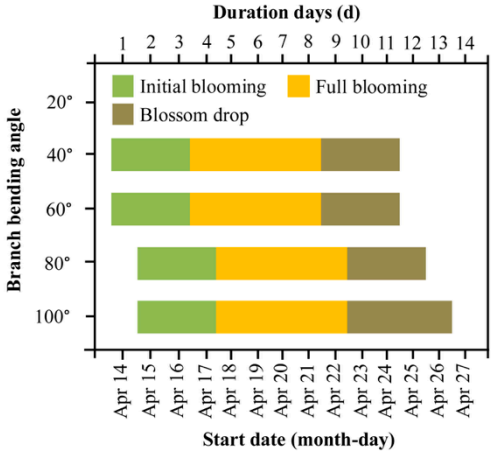

Figure 1. Flowering phenology of Korla fragrant pear at four branch-bending angles. Initial bloom (5% open flowers), full bloom (25–75% open flowers) and petal fall (75–95% petals dropped) were monitored daily from 14 to 26 April 2022. The data are presented as the duration (days) of each phase. Different lowercase letters above the bars indicate significant differences among treatments (Duncan's test, $P < 0.05$).

2.2. Impact of Branch Bending Angle on the Flowering Rate and Fruit Set of Korla Fragrant Pear

The flowering rate (flowering buds/total buds) and fruit set (retained fruits after the first physiological drop/thinned flowers) were recorded from April–May 2023. The 40° angle resulted in the lowest flowering rate ($P < 0.05$ versus all the other angles); the values did not differ between 60–100°, where 100° reached 7.89%. Fruit set peaked at 80° (11.77%), followed by 100° (8.66%), and both exceeded 40° and 60° ($P < 0.05$). Thus, 80° pulling optimized the fruit set, whereas the flowering rate was suppressed only at 40°.

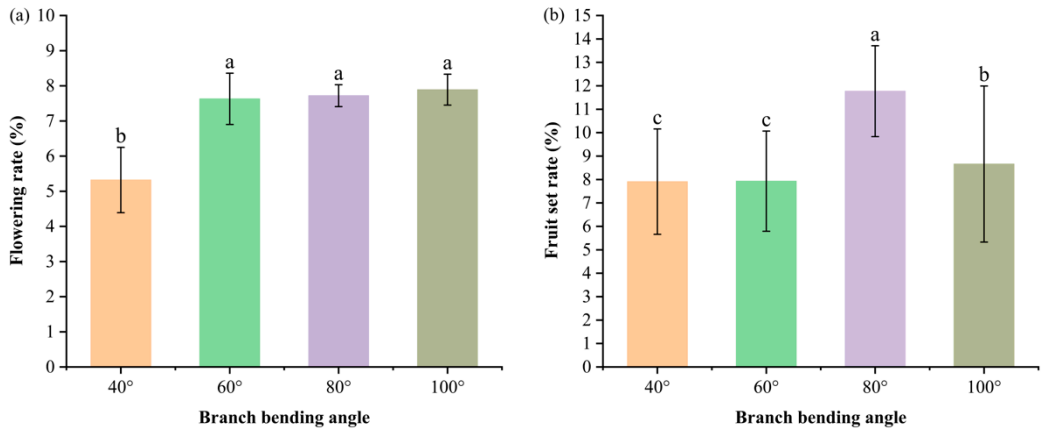

 doi:10.20944/preprints202512.2343.v1

Figure 2. Flowering rates (a) and fruit set rates (b) of Korla fragrant pears with different branch-bending angles. The data are presented as the means ± SEs; n = 5 branches per angle. Different letters above the bars denote significant differences (Duncan's test, $P < 0.05$).

2.3. Impact of Branch Bending Angle on Leaf Morphology, Chlorophyll Content and Mineral Composition of Korla Fragrant Pear

To test whether branch orientation alters source-leaf morphology, photosynthetic potential and mineral supply capacity, we determined single-leaf fresh mass, dry mass, area, linear dimensions, chlorophyll pigments and mineral element concentrations across the four bending angles.

The leaf morphology data revealed that moderate bending (60–80°) significantly increased all the growth metrics: 80° resulted in the greatest single-leaf fresh mass (1.25 g), the heaviest dry mass (0.53 g) and the greatest leaf area (59.51 cm²), all of which were significantly greater than those at 40° and 100° ($P \leq 0.05$), whereas 60° ranked second and 40°/100° presented the smallest values (Figure 3a).

The chlorophyll content mirrored the morphological response; at 80°, the chlorophyll a, chlorophyll b and total chlorophyll (a+b) contents reached 2.53, 0.58 and 3.11 mg g^{-1}, respectively—significantly higher than those in all the other treatments ($P \leq 0.05$), whereas the SPAD values showed the same numerical trend (36.52 at 80°), but the values did not significantly differ ($P > 0.05$), indicating a visually greener yet statistically comparable photosynthetic unit under moderate bending (Figure 3b).

Leaf mineral profiling (Figure 3c) revealed that the 80° pulling treatment modified the macronutrient and micronutrient concentrations: the concentration of nitrogen reached 23.36 mg/g, which was significantly greater than that at 40° (20.42 mg/g) and 100° (19.42 mg/g) ($P \leq 0.05$) but not different from that at 60° (22.36 mg/g) ($P > 0.05$); the concentration of magnesium peaked at 46.43 mg/g, which was significantly greater than that at 40° (44.86 mg/g) and 60° (44.88 mg g^{-1}) ($P \leq 0.05$) but was comparable to that at 100° (47.94 mg/g) ($P > 0.05$); the concentration of copper was greatest at 23.64 mg g^{-1}, which exceeded all the other angles ($P \leq 0.05$); the concentrations of iron (25.87 mg/g) and calcium (5.14 mg/g) did not differ significantly from those at any angle ($P > 0.05$); and the concentration of zinc (42.53 mg/g) was significantly lower than that at 60° (48.27 mg/g) ($P \leq 0.05$) but not significantly different from that at 40° (38.04 mg/g) and 100° (40.59 mg/g) ($P > 0.05$). Overall, the 80° pulling treatment elevated leaf N, Mg and Cu availability, increasing the source capacity for fruit development.

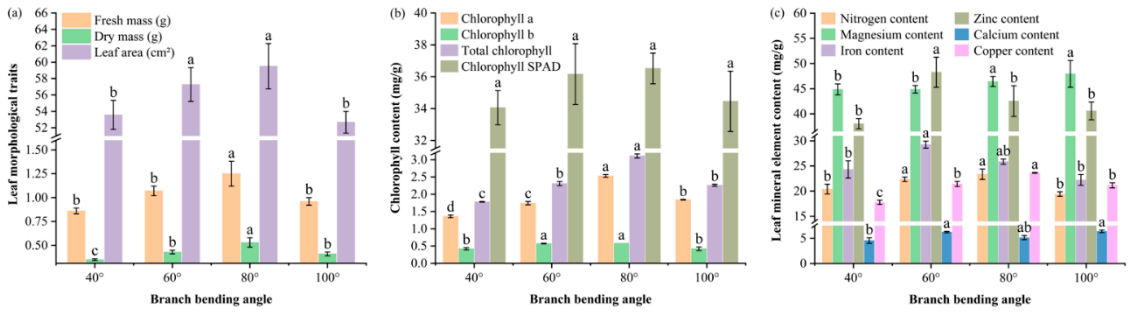

Figure 3. Leaf morphology, chlorophyll content and mineral element concentrations of Korla fragrant pear at four bending angles. (a) Single-leaf fresh mass, dry mass and area; the Y-axis is broken between 1.6 and 51 to better visualize differences. (b) Chlorophyll a, chlorophyll b, total chlorophyll and total chlorophyll SPAD; the Y-axis is broken between 3.2 and 31.5 mg/g. (c) Nitrogen, magnesium, iron, zinc, calcium and copper; the Y-axis is broken between 7.5 and 14 mg/g and between 31 and 36.5 mg/g. Mean ± SE, n = 5 leaves per angle. Different letters indicate significant differences (Duncan's test, $P < 0.05$).

 doi:10.20944/preprints202512.2343.v1

2.4. Impact of Branch Bending Angle on Fruiting Shoot Typology

To evaluate whether branch angle reallocates assimilates by modifying fruiting architecture, we classified spur types and measured the corresponding branch dimensions across the four bending angles.

Fruiting-shoot composition (Figure 4a) revealed that pulling ≥ 60° significantly mitigated shoot vigor and rebalanced vegetative vs. reproductive competition. Compared with the 40° treatments, the 60°, 80° and 100° treatments collectively increased the combined share of short plus medium spurs and reduced the proportion of long spurs. The short-spur percentage was greatest at 60° (26.9%), followed by 80° (18.8%) and 100° (18.5%), which were significantly greater than 40° (15.1%) ($P \leq 0.05$). The medium-spur percentage peaked at 80° and 100° (41.1% and 41.5%, respectively), significantly exceeding 40° (25.3%) and 60° (35.9%) ($P \leq 0.05$). The long-spur proportion at 60°, 80° and 100° (~37–40%) was significantly lower than that at 40° (59.6%) ($P \leq 0.05$), with no difference among the three larger angles ($P > 0.05$).

The branch dimension traits indicated that short-spur length did not differ significantly among the angles ($P > 0.05$), whereas the medium-spur length at 80° (9.50 cm) was significantly shorter than that in the other three treatments ($P \leq 0.05$), and the long-spur length at 80° (47.3 cm) was significantly greater than that at 40°, 60° and 100° ($P \leq 0.05$) (Figure 4b). The short-spur basal diameter at 60°, 80° and 100° (≥ 0.83 cm) was significantly greater than that at 40° (0.67 cm) ($P \leq 0.05$). The medium-spur diameter peaked at 80° (1.43 cm) but was not significantly different from the other angles ($P > 0.05$). The long-spur diameter was greatest in the 80° treatment (1.54 cm), significantly exceeding that in all the other treatments ($P \leq 0.05$) (Figure 4c).

Thus, the 80° pulling treatment restructured the canopy into shorter but thicker fruiting spurs, creating more efficient "unloading ports" that reconcile vegetative vigor with reproductive sink strength.

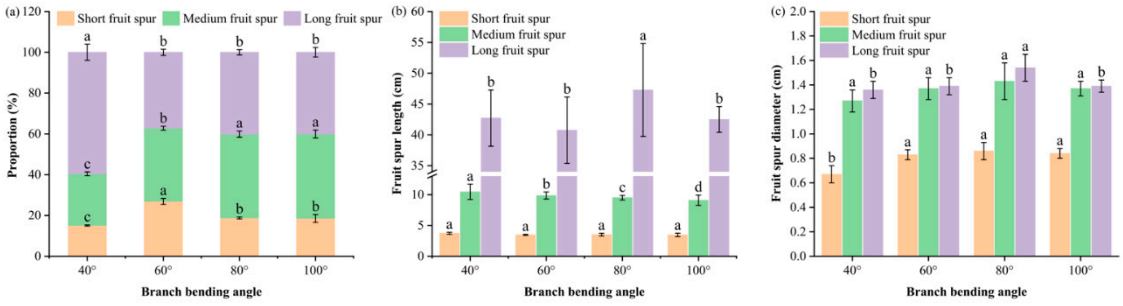

Figure 4. Fruiting-shoot typology and branch-dimensional traits of Korla fragrant pear under four branch-bending angles: (a) proportions of short (< 5 cm), medium (5–15 cm) and long (> 15 cm) fruiting spurs**.** (b) Fruit spur length; the **Y-axis is broken between 13 and 34 cm to better visualize differences.** (c) Fruit spur diameter. Mean ± SE, n = 5 branches per angle. Different letters indicate significant differences (Duncan's test, $P < 0.05$).

2.5. Impact of Branch Bending angle on Branch Water Status and Nitrogen Reserve

To test whether the bending angle affects the water–nitrogen coupling that underpins subsequent fruit development, we quantified the xylem/phloem water content, tissue ratio and total nitrogen across branch segments.

Branch water partitioning (Figure 5a) revealed that the 80° pulling treatment significantly decreased the total branch water content to 56.2% compared with 40° (63.1%) and 60° (65.1%) ($P \leq 0.05$), whereas no difference was detected compared with 100° (57.2%) ($P > 0.05$). The phloem water content under 80° (21.5%) was also significantly lower than that under 40° and 60° ($P \leq 0.05$) but remained comparable to that under 100° ($P > 0.05$).

The xylem-to-phloem dry weight ratio (Figure 5b) peaked at 1.78 under 80°, which was significantly greater than 40° (1.68) ($P \leq 0.05$) and statistically equivalent to 60° (1.77) and 100° (1.76)

 doi:10.20944/preprints202512.2343.v1

(P > 0.05), indicating a "drier but better proportioned" hydraulic architecture that limits lignin deposition while maintaining sugar-transport capacity.

The tissue nitrogen reserves (Figure 5c) were highest for total branch N at 40° (29.40 ± 3.56 mg g^{-1} DW), which were significantly greater than those at 60°, 80° and 100° (22–24 mg g^{-1} DW) ($P \leq 0.05$), with no significant differences among the latter three (P > 0.05). Thus, 40° provided the greatest nitrogen reservoir within the branch, while larger bending angles maintained a lower but statistically equivalent N pool.

Taken together, 80° bending establishes a water-restricted yet nitrogen-adequate branch framework that prevents hydraulic overload while supplying sufficient mineral nutrients, creating a physiological precondition for premium fruit formation.

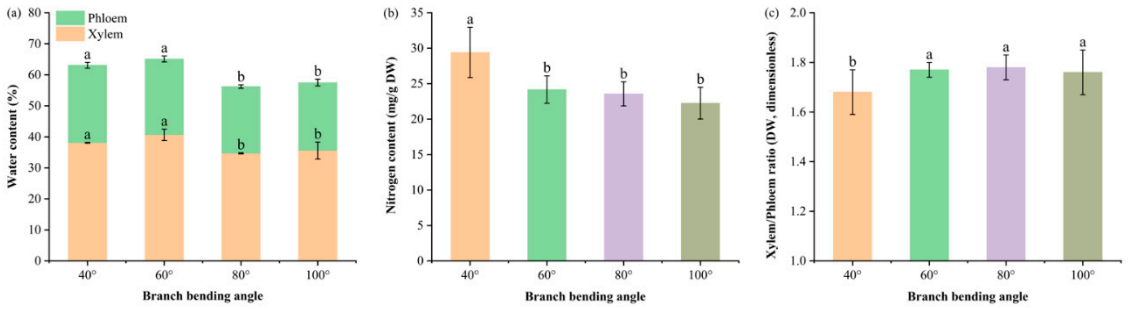

Figure 5. Water content in the xylem and phloem, branch nitrogen concentration and dry weight ratio of the xylem to phloem of Korla fragrant pear under four branch-bending angles: (a) Stacked water content of the xylem and phloem; letters above segments indicate significant differences within the same tissue (Duncan's test, P < 0.05). Total water content: 40° = 63.1% (a), 60° = 65.1% (a), 80° = 56.2% (b), 100° = 57.2% (b); letters in parentheses denote total-water comparison. (b) Total nitrogen concentration in the whole branch. (c) Xylem-to-phloem dry-weight ratio. Mean ± SE, n = 3 branches per angle. Different letters indicate significant differences (Duncan's test, P < 0.05).

2.6. Impact of Branch Bending Angle on the Nutrient Contents of Korla Fragrant Pear Buds

To test whether the superior fruit set and calyx removal observed at 80° and 60°, respectively, stem from enhanced carbon/nitrogen build-up in the buds, we determined the soluble sugar and total nitrogen concentrations at the green-cluster stage.

Bud nutrient profiling (Figure 6a) revealed that bending angles between 60° and 80° promoted the accumulation of both soluble sugars and nitrogen, with carbon accumulation being more responsive than nitrogen accumulation.

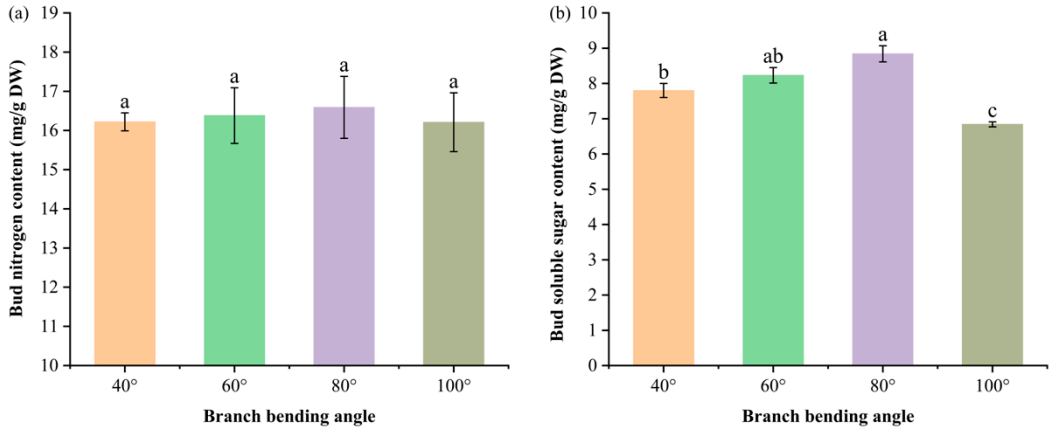

 doi:10.20944/preprints202512.2343.v1

Figure 6. Bud nitrogen and soluble sugar contents of Korla fragrant pear at four branch-bending angles: (a) nitrogen content; (b) soluble sugar content. Mean ± SE, n = 5 bud replicates per angle. Different letters indicate significant differences (Duncan's test, $P < 0.05$).

The soluble sugar content (Figure 6b) peaked at 80° (8.84 mg g^{-1} DW), which was significantly greater than that at 40° (7.80 mg g^{-1} DW) and 100° (6.84 mg g^{-1} DW) ($P \leq 0.05$) and comparable to that at 60° (8.23 mg g^{-1} DW) ($P > 0.05$). Total nitrogen was highest at 80° (16.59 mg g^{-1} DW) but did not differ significantly among the angles ($P > 0.05$). Consequently, the C:N ratio was maximized under 80°, favoring flower bud differentiation and subsequent fruit set.

Taken together, moderate pulling (60–80°) enhances bud carbon status while maintaining adequate nitrogen, providing a biochemical basis for the greater fruit set observed at 80°.

2.7. Impact of Branch Bending Angle on Endogenous Hormone Dynamics in Young Fruits at Key Stages of Calyx Abscission and the First Physiological Fruit Set of Korla Fragrant Pear2.7

To elucidate the hormonal mechanisms underlying angle-dependent fruit set, we monitored ten endogenous hormones in young 'Zhongai No. 1' dwarf interstock from April 19 to May 4—a critical window spanning calyx abscission and the first period of physiological fruit drop. Hormone profiling was performed using LC–MS/MS to explore potential associations between branch bending angles and the patterns of calyx shedding and fruit set.

Gibberellin A_1 (GA_1) remained below the detection limit until 28 April, when it surged transiently: 100° peaked at 3.74 ng/g DW, significantly higher than the other angles ($P \leq 0.05$), and then fell rapidly toward a low plateau by 4 May. On 1 May, 80° rebounded to 2.27 ng/g DW, surpassing 60° ($P \leq 0.05$), whereas 60° ultimately took the lead at 2.23 ng/g DW on 4 May ($P \leq 0.05$). The radar profile (Figure 7b) illustrates this hand-over: 100° dominates the late-April apex, 80° decreases to the bottom segment, and 60° emerges as the final peak.

Gibberellin A_3 (GA_3) followed a "low–spike–decline" trajectory, with only a transient elevation at 40° on 25 April before it returned to baseline levels across all the angles. The multi-index radar profile (Figure 7d) visualizes these dynamics: 80° presents a low-and-flat band throughout; 60° follows an "early-high, then-fading" arc; and 40° and 100° occupy mid-peak sectors on 25 and 28 April, respectively, with 100° showing a "low-to-high" rebound trajectory and 40° maintaining elevated levels after its peak.

Gibberellin A_4 (GA_4) exhibited a "rise–peak–decline" pattern at 60° and 80°, peaking on 28 April at 58.4 ng/g DW and 50.6 ng/g DW, respectively—both significantly higher than 40° and 100° ($P \leq 0.05$)—before it reached baseline. In contrast, 40° and 100° showed a steady downward trend after early April; only 100° displayed a minor late rebound to 21.5 ng/g DW on 4 May. The radar profile (Figure 7f) mirrors this divergence: 60°/80° occupies the late-April apex sector, whereas 40° remains low and 100° traces a gentle "low-to-high" tail. and 100° traces a gentle "low-to-high" tail.

Gibberellin A_7 (GA_7) showed a "rise–peak–decline" pattern at 60° and 80°, peaking on 28 April at 1.44 ng/g DW and 1.34 ng/g DW, respectively—both significantly higher than 40° and 100° ($P \leq 0.05$)—before it returned to baseline. In contrast, 40° remained essentially flat throughout, whereas 100° remained low until a sharp decrease on 4 May. The radar profile (Figure 7h) captures this divergence: 60°/80° dominates the late-April apex sector, 40° traces a low horizontal band, and 100° displays a terminal "cliff" descent.

Indole-3-acetic acid (IAA) showed a "flat–surge–decline" trend at 40°, 60° and 100°, whereas 80° followed a "flat–surge–plateau" pattern (Figure 8a). Before 28 April, 80° and 60° were significantly lower than 40° and 100° ($P \leq 0.05$); thereafter, 80° continued to rise and plateaued at 2.05 ng/g DW on 4 May, remaining significantly higher than all the other angles at the final two samplings ($P \leq 0.05$). In contrast, 40°, 60° and 100° peaked on approximately 28 April or 1 May and decreased markedly by 4 May; the minimum value (0.62 ng/g DW) was recorded at 60°. The radar plots (Figure 8b) mirror the late-phase dominance of 80°.

 doi:10.20944/preprints202512.2343.v1

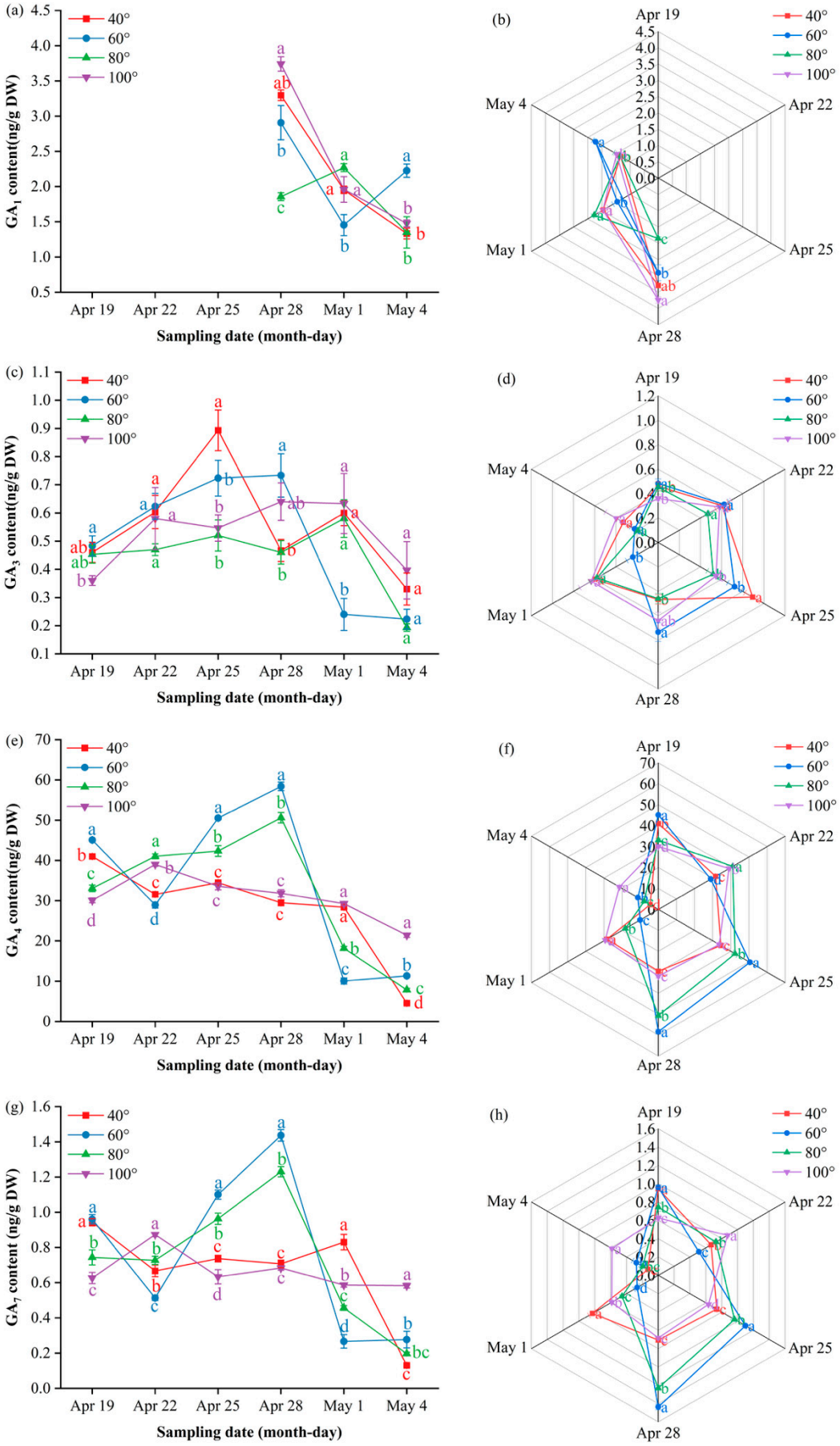

 doi:10.20944/preprints202512.2343.v1

Figure 7. Dynamic GA content and multi-index radar profile comparison: (a) changes in the GA_1 content of Korla fragrant pear young fruits at key sampling stages under different branch bending angles; (b) GA_1 multi-index radar profile; (c) changes in the GA_3 content; (d) GA_3 multi-index radar profile; (e) changes in the GA_4 content; (f) GA_4 multi-index radar profile; (g) changes in the GA_7 content; (h) GA_7 multi-index radar profile. Mean ± SE, n = 3 biological replicates. Different letters indicate significant differences among the angles on the same sampling date (Duncan's test, $P < 0.05$).

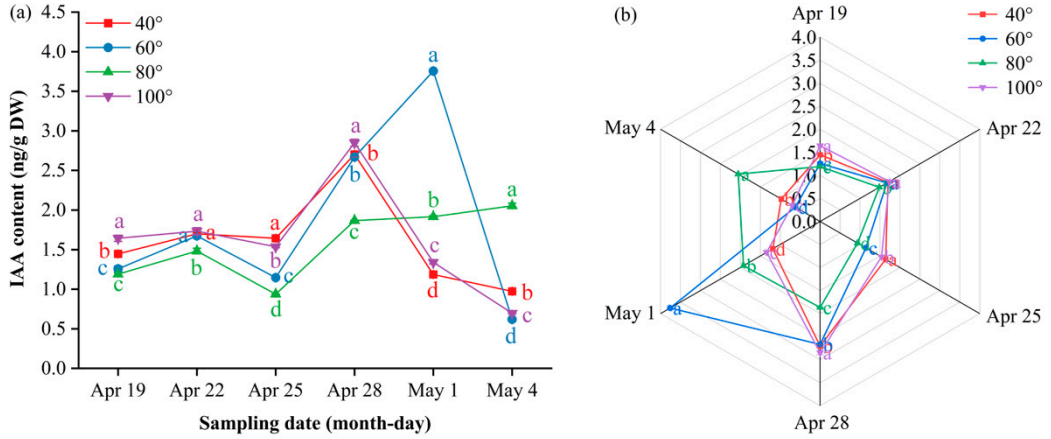

Figure 8. Dynamic IAA content and multi-index radar profile comparison. Figure 3 (a) Changes in the IAA content of Korla fragrant pear young fruits at key sampling stages under different branch bending angles; (b) radar profile of multiple indices for the four angles. Mean ± SE, n = 3 biological replicates. Different letters indicate significant differences among the angles on the same sampling date (Duncan's test, $P < 0.05$).

Cis- and trans-zeatin in the 80° treatment followed a "slow-rise–steep-rise" two-phase pattern: levels remained low to moderate from 19 to 28 April but then increased rapidly to simultaneous peaks on 4 May (CZ 0.27 ng/g DW; TZ 0.29 ng/g DW), which were significantly greater than 40° and 60° ($P \leq 0.05$) but still lower than 100°. The 40° angle displayed an overall upward trend, with two distinct peaks on 25 April and 4 May, whereas 60° and 100° peaked on 1 May and then declined. The radar profiles (Figure 9b,d) show 100° as the outermost sector on 1 May, 40° as it exhibited dual protrusions on 25 April and 4 May, and 80° as it expanded only on 4 May, confirming the angle × time interaction.

Abscisic acid (ABA) exhibited a "surge–decline" pattern (Figure 10a). Before 28 April, 80° remained in the inner ring of the radar plot, with concentrations significantly lower than those reached later ($P \leq 0.05$). The values then increased, peaking on 28 April at 2058 ng/g DW at 80° and significantly higher than those at 60°, 100° and 40° ($P \leq 0.05$); this dominance persisted on 1 May (1451 ng/g DW). Thereafter, the levels decreased; on 4 May, they ranked 60° (1274 ng/g DW) > 40° (757 ng/g DW) > 80° (609 ng/g DW) > 100° (446 ng/g DW) ($P \leq 0.05$). Radar plots (Figure 10b) show 80° at the outermost arc on 28 April and 1 May, whereas 60° expands to the periphery only on 4 May, illustrating the sequential shift in ABA dominance during calyx abscission.

Salicylic acid (SA) dynamics split into two clear tracks (Figure 11a). The high-angle group (80°, 100°) climbed steadily until 1 May, peaking simultaneously at 15.48 ng/g DW (80°) and 12.85 ng/g DW (100°), each significantly higher than 40° ($P \leq 0.05$), and then declined sharply; by 4 May, both had fallen to their respective minima—13.32 ng/g DW for 80° and 11.59 ng/g DW for 100°—which were significantly lower than 40° and 60° ($P \leq 0.05$). The low-angle group (40°, 60°) showed divergent paths: 40° bottomed out on 25 April (6.86 ng/g DW, $P \leq 0.05$) before rising continuously to 15.18 ng/g DW on 4 May, whereas 60° increased almost linearly to the overall maximum of 18.68 ng/g DW on 4 May ($P \leq 0.05$). Consequently, 60° maintained the highest SA level across the window, with 80° holding second place until 1 May. The radar plots (Figure 11b) mirror this switch: from 22 April onward, 60° and 80° occupy the outer rings, whereas 40° and 100° stay closer to the center; on 1 May,

 doi:10.20944/preprints202512.2343.v1

the 80° sector reaches its maximum outward extension, and by 4 May, only 60° expands to the periphery, visually underlining the angle- and time-specific SA burst during calyx abscission.

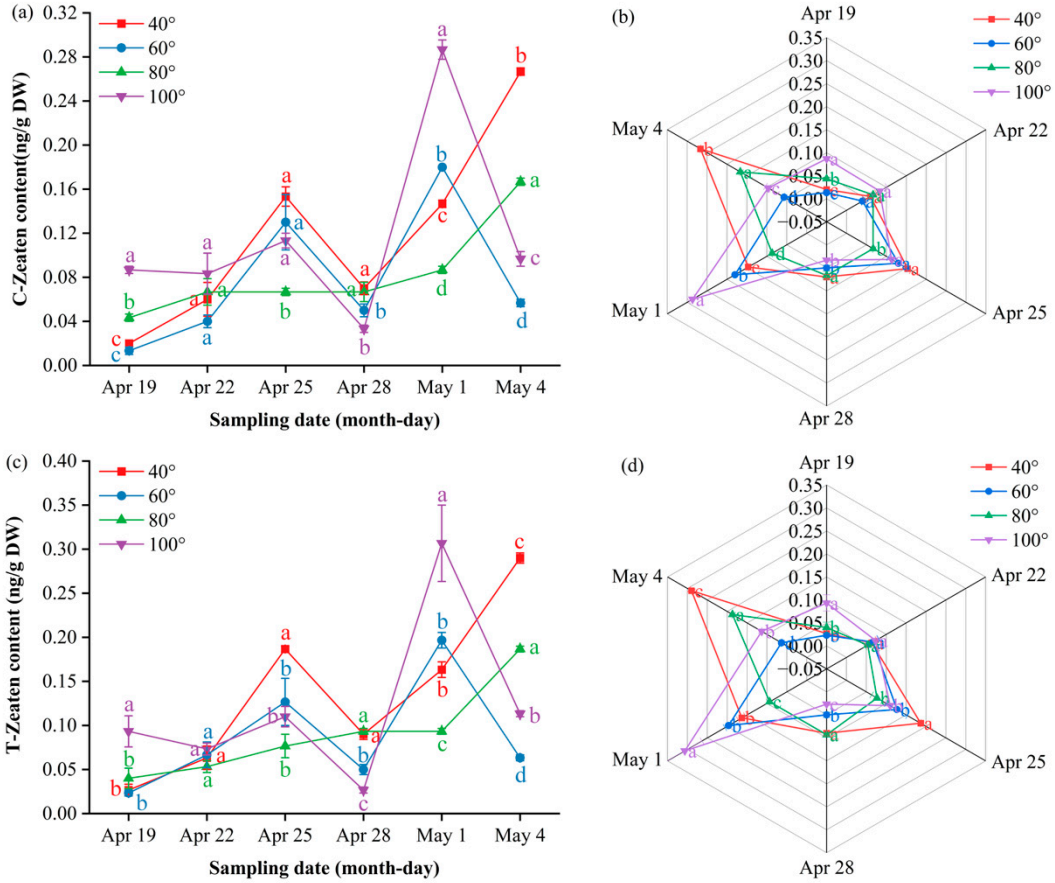

Figure 9. Dynamic cytokinin content and multi-index radar profile comparison: (a) changes in the cis-zeatin content of Korla fragrant young pear fruits at key sampling stages under different branch bending angles; (b) cis-zeatin multi-index radar profile; (c) changes in the trans-zeatin content; (d) trans-zeatin multi-index radar profile. Mean ± SE, n = 3 biological replicates. Different letters indicate significant differences among the angles on the same sampling date (Duncan's test, $P < 0.05$).

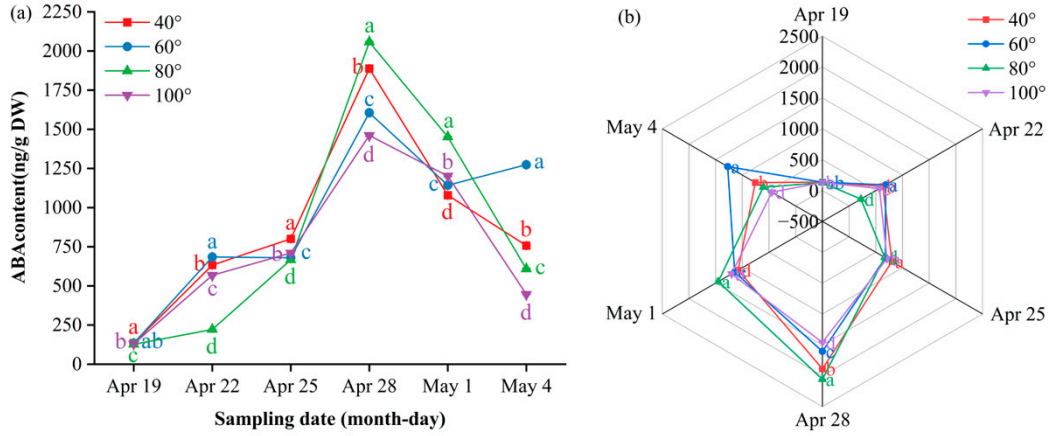

Figure 10. Dynamic ABA content and multi-index radar profile comparison: (a) changes in the ABA content of Korla fragrant pear young fruits at key sampling stages under different branch bending angles; (b) ABA multi-index radar profile. Mean ± SE, n = 3 biological replicates. Different letters indicate significant differences among the angles on the same sampling date (Duncan's test, $P < 0.05$).

 doi:10.20944/preprints202512.2343.v1

Jasmonic acid (JA) displayed a "flat–surge" pattern at 40°, 80° and 100° and a "flat–surge–decline" pattern at 60° (Figure 11c). Basal concentrations ≤ 30 ng/g DW were maintained until 28 April, after which all the angles rose rapidly. On 1 May, the peak appeared at 60° at 622.8 ng/g DW, with 80° in second place at 213.6 ng/g DW, which were significantly greater than those at 100° (131.6 ng/g DW) and 40° (106.6 ng/g DW) ($P \leq 0.05$). Thereafter, 60° declined sharply, while the remaining angles continued to increase; by 4 May, the ranking was 80° (341.0 ng/g DW) > 40° (200.7 ng/g DW) > 100° (159.1 ng/g DW) > 60° (93.5 ng/g DW), with significant differences between each step ($P \leq 0.05$). Overall, 80° maintained a consistently high level throughout the window. Radar plots (Figure 11d) show 80° occupying the outermost arc from 22 April onward, whereas 40° and 100° remain closer to the center, visually confirming the angle- and time-dependent JA burst during calyx abscission.

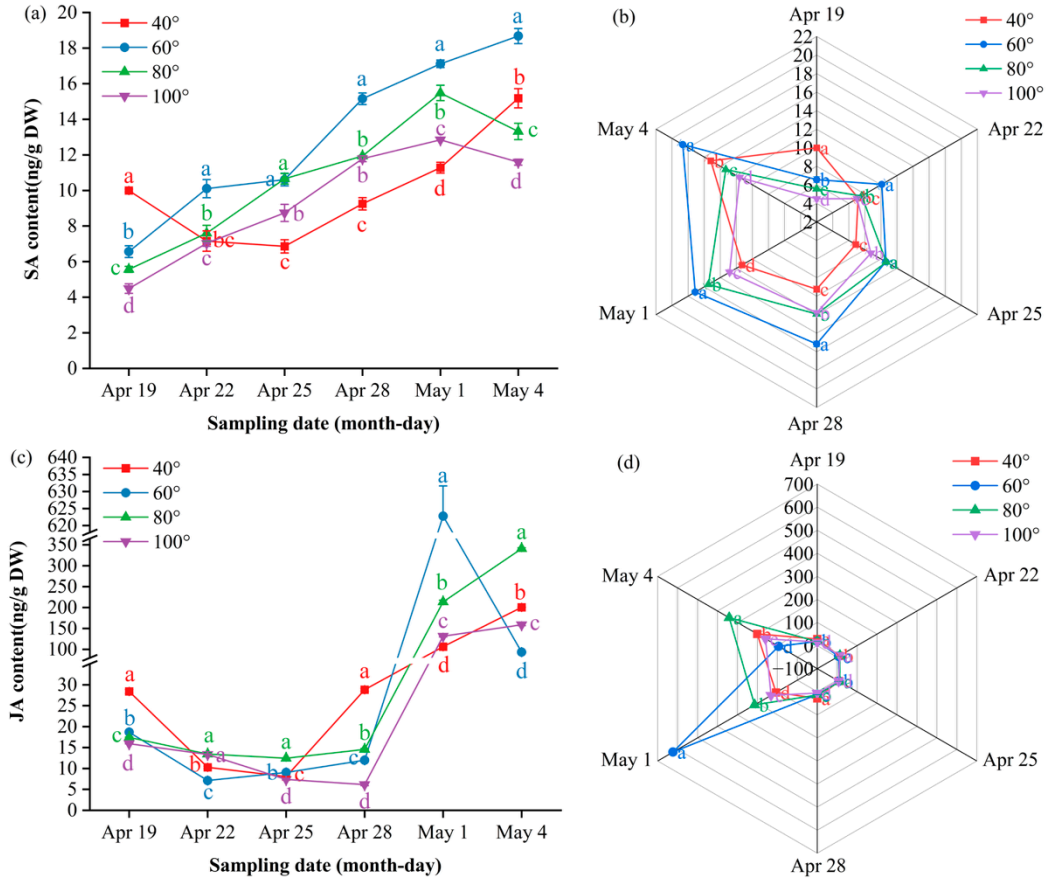

Figure 11. Dynamic salicylic acid (a, b) and jasmonic acid (c, d) contents of Korla fragrant pear young fruits at key sampling stages under different branch-bending angles. (a, c) Time-course changes; (b, d) multi-index radar profiles. Mean ± SE, n = 3 biological replicates. Different letters indicate significant differences among the angles on the same sampling date (Duncan's test, $P < 0.05$).

April 28 served as the pivotal hormonal switch point. Before this date, low levels of IAA and zeatin (cis-/trans-zeatin) permitted calyx abscission, whereas simultaneous surges of GA_4, GA_7, ABA, SA and JA initiated separation. After 28 April, the levels of these hormones decreased rapidly, whereas those of IAA and zeatin increased steadily and peaked on 1–4 May; this "second wave" reinforced ovary IAA–zeatin signaling, antagonizing ABA-induced abscission reactivation and thus reducing the first degree of physiological fruit drop. Concentrations >0.30 ng g^{-1} DW risk reactivating cell division, promoting fruit enlargement and increasing persistent calyx fruits. The 80° bending angle precisely maintained the zeatin concentration at 0.27–0.29 ng g^{-1} DW, combined with high levels of soluble sugars and IAA, minimized calyx retention and maximized fruit set (11.8%), providing a practical physiological basis for high-density Korla fragrant pear orchards.

 doi:10.20944/preprints202512.2343.v1

2.8. Impact of Branch Bending Angle on Consumer-Grade Fruit Quality

Harvest measurements revealed that the bending angle significantly modified both external and internal quality traits (Figures 12 and 13).

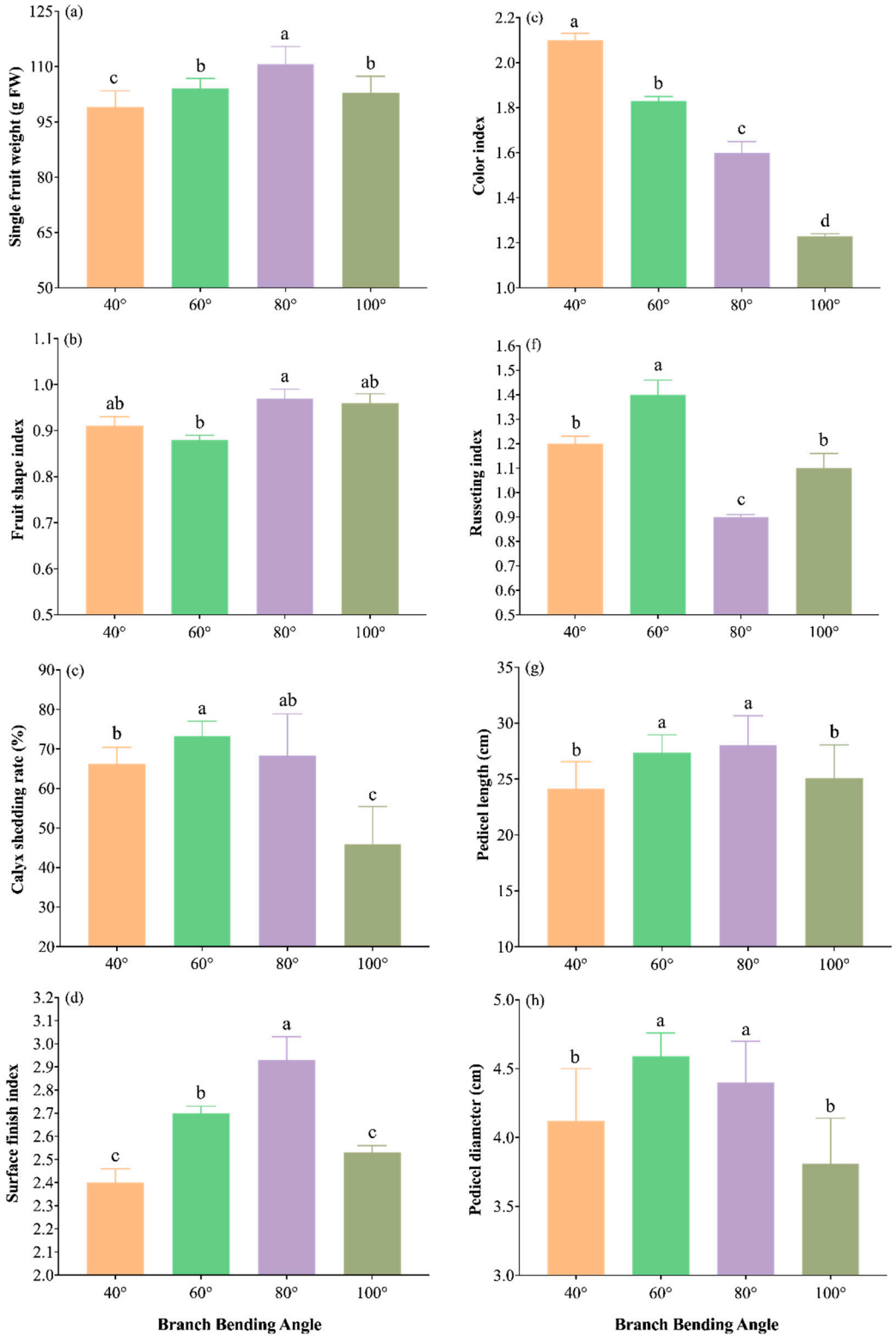

Figure 12. External fruit quality traits of Korla fragrant pear under four branch-bending angles: (a) single-fruit weight, (b) fruit shape index, (c) calyx shedding rate, (d) surface finish index, (e) color index, (f) russeting index,

 doi:10.20944/preprints202512.2343.v1

(g) pedicel length, and (h) pedicel diameter. Mean ± SE, n = 30 fruit per angle. Different letters indicate significant differences (Duncan's test, $P < 0.05$).

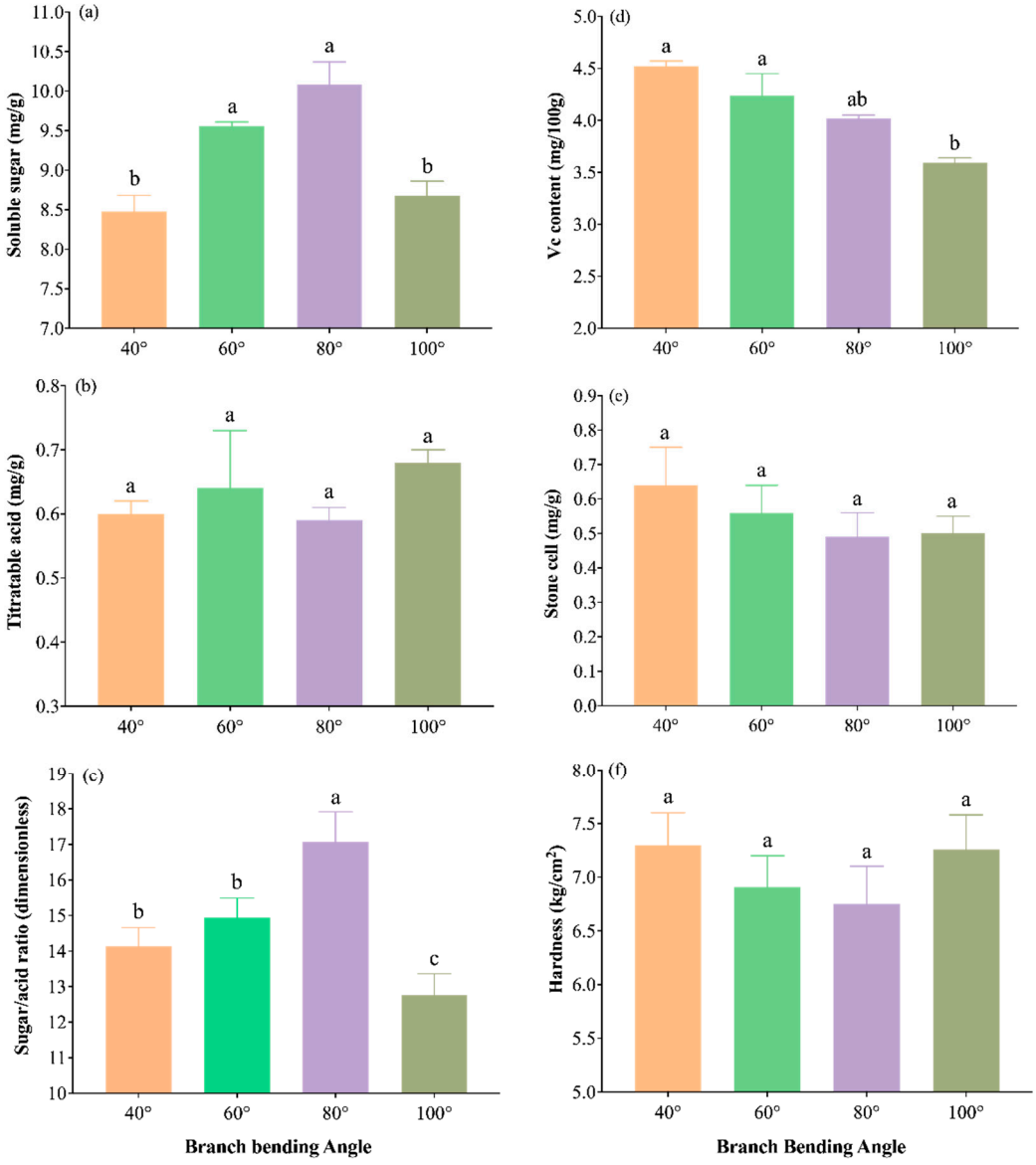

Figure 13. Internal fruit quality traits of Korla fragrant pear under four branch-bending angles: (a) sugar/acid ratio, (b) soluble sugar content, (c) titratable acid content, (d) vitamin C content, (e) stone-cell content, and (f) hardness. Mean ± SE, n = 30 fruit per angle. Different letters indicate significant differences (Duncan's test, $P < 0.05$).

The external quality traits are summarized in Figure 12a–h. The 80° treatment produced the heaviest fruit (110.7 g), significantly outweighing all the other angles ($P \leq 0.05$). Calyx removal under 80° (71%) was statistically comparable to the maximum in 60° (73%, $P > 0.05$), ensuring a smooth shoulder. The shape index peaked at 0.97 under 80°, whereas the peel smoothness (cleaning index of 2.93) was the highest, and the color uniformity (rust index of 0.90) was intermediate—higher than 100° but lower than 40° and 60°—yielding the most attractive overall finish. Additionally, 80° yielded the longest pedicel (28.0 cm) and thickest stalk base (4.40 mm), which were significantly greater than those of 40° and 100° ($P \leq 0.05$). Overall, 80° delivers the largest, cleanest and most uniformly finished fruit, providing a clear market advantage for high-density Korla fragrant pear production.

 doi:10.20944/preprints202512.2343.v1

The internal quality indices are shown in Figure 13a–f. The 80° treatment resulted in the highest soluble-sugar content (10.08 mg g^{-1}), significantly outperforming 40° and 100° ($P \leq 0.05$) but being comparable to 60° ($P > 0.05$); it also resulted in the highest sugar/acid ratio (17.08), which was significantly greater than that at all the other angles ($P \leq 0.05$). Titratable acid was lowest under 80° (0.59 mg g^{-1}), with no significant interangle differences ($P > 0.05$), indicating the best sugar–acid balance. The vitamin C concentration reached 4.02 mg $(100\ g)^{-1}$, the stone-cell content was lowest (0.49 mg g^{-1}), and the flesh hardness was minimal (6.75 kg cm^{-2}); all three traits were statistically similar across treatments ($P > 0.05$) but were numerically optimal under 80 °C. Overall, 80° pulling resulted in the highest sugar/acid ratio and the finest taste potential, providing the best internal quality for high-density Korla fragrant pear orchards.

Taken together, the results indicate that the 80° bending angle consistently yields the heaviest, cleanest and most balanced fruit, with the highest sugar/acid ratio, lowest stone-cell burden and optimal external finish, providing an integrated quality advantage that directly translates into higher market value and consumer preference for high-density Korla fragrant pear orchards. The radar fingerprint (Figure 14) places the 80° polygon at the outermost arc for both external (single-fruit weight, calyx removal, surface finish index) and internal (soluble sugar, sugar/acid ratio) traits, corroborating its superior combined quality among all the angles.

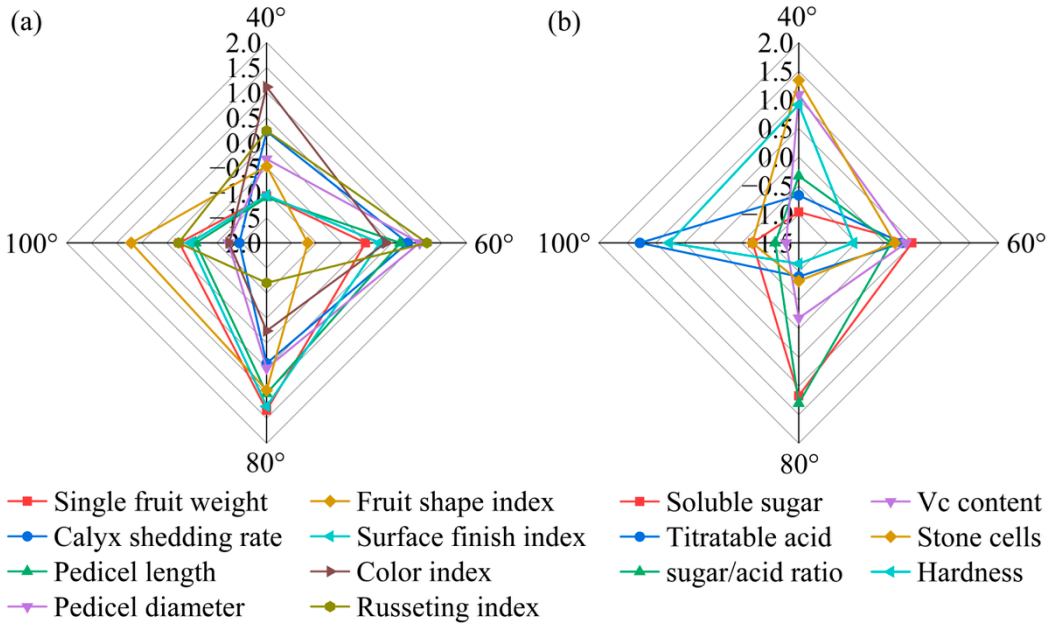

Figure 14. Comparison of external and internal fruit quality indices of Korla fragrant pear under four branch-bending angles: (a) standardized external-quality indices (Z scores); (b) standardized internal-quality indices (Z scores). Mean ± SD, n = 30 fruit per angle. The error bars and significance letters are presented in Figures 6 and 7, respectively.

2.9. Pixel-Level Dissection of the Correlation Heatmap

To visually reveal the coordinated variation patterns of physiological traits under different branch-bending angles, a Pearson correlation matrix was constructed from 57 indices and dissected at the pixel level (Figure 16). By interpreting hue and saturation in microregions, seven biologically meaningful chromatic patterns were identified:

① **Early-Hormone Response Band (Columns 1–10)**

GA_4-E, GA_7-E, and ABA-E formed a continuous warm-colored band under the 60° and 80° treatments, with the **80° treatment** showing the deepest color value (strongest positive correlation) and 60° appearing orange–red. In contrast, 40° and 100° shifted to cyan–blue. This finding indicates

 doi:10.20944/preprints202512.2343.v1

that the carbon–nitrogen–hormone synergy was strongest in the 60–80° range and diminished rapidly at more acute or obtuse angles.

② **Temporal Gradient (Rowwise Scan)**

Each hormone row exhibited a temporal gradient from early (E) to late (L) phases, transitioning from red to blue. The **80° treatment** resulted in the steepest color step (spanning approximately three hue levels), whereas the 40° treatment resulted in only approximately one level, suggesting that the 80° angle produced the sharpest hormone half-life turnover and most distinct physiological rhythm.

③ **Carbohydrate Enrichment Band (Columns 11–12)**

The soluble sugar pixel reached the maximum red intensity under the **80° treatment**, remained orange–red at 60°, and turned light blue at 40° and 100°. The bud nitrogen pixel remained warm-orange across all angles, with only marginally deeper red at 80° versus 60°. Thus, the carbon peak was visually localized at 80°, whereas nitrogen remained in the same warm tier across 60–80°.

④ **Leaf Economics Spectrum (Columns 13–22)**

Chlorophyll a, b, and total pixels formed a red plateau under 60–80°, whereas 40° and 100° decreased to green. The identical warm pattern in terms of leaf nitrogen confirmed the "larger-greener-richer" leaf cluster, specifically at 60–80°.

⑤ **Fruiting-Shoot Architecture Mosaic (Columns 23–34)**

ShortRate and MediumRate pixels produced a bell-shaped warm band centered at 60–80° (60° orange, 80° red, 40° cyan, 100° light green). The medium-thick pixels followed the same bell, but the **80° treatment** resulted in the deepest red color. Therefore, the thickest medium spurs colocalized with the warm band, not uniquely at 80°.

⑥ **Branch Water–Nitrogen Coupling Block (Columns 35–40)**

Both the xylem-to-phloem dry-weight ratio and branch nitrogen pixels displayed the darkest red under the **80° treatment**, orange at 60°, and blue at 40° and 100°. The visual peak lies at 80°, forming an "optimal–suboptimal" continuum with 60°.

⑦ **Consumer-Quality Tail (Columns 41–57)**

The stone-cell pixel was blue under **80°**, light blue at 60°, pink at 40°, and orange at 100°, indicating that low stone-cell content was visually bracketed within the 60–80° range. The fruit-set-rate pixel reached a maximum absorbance in the red spectrum at 80° and turned cyan at 100°, while 60° remained in the warm tier.

Overall, the color field converts >1,000 measurements into a bell-shaped warm domain centered at 60–80° that spans hormones, carbon, leaf economics, spur thickness, stone cells, and final fruit set, whereas 40° and 100° are separated by cooler hues.

2.10. Multivariate Analysis and Angle Optimization

To objectively identify the optimal branch-bending angle, **57 phenotypic, physiological, and quality traits** from the correlation matrix were integrated via principal component analysis (PCA). Three principal components (PC1–PC3) were extracted, collectively explaining 100% of the total variance (Table 1). PC1 (47.34%) was primarily driven by the soluble sugar content, GA_1, and flowering rate; PC2 (32.01%) was driven by ABA, GA_1, and SA; and PC3 (20.64%) was driven by the fruit set rate and nitrogen content (Table 2).

On the basis of the PCA scores, a comprehensive evaluation index (D) was calculated using the membership function method, weighted by the variance contribution rates of the PCs. The D-value ranking was **80° (0.718) > 60° (0.687) > 40° (0.317) > 100° (0.197)** (Table 3), confirming that 80° pulling achieved the best overall performance.

The PCA biplot (Figure 16) revealed trait–angle relationships: the 80° treatment was positioned in the positive PC1 direction and closely associated with higher soluble sugar, GA_4, GA_7, and fruit set rates, whereas the 100° treatment aligned with the titratable acid content and leaf Mg content.

 doi:10.20944/preprints202512.2343.v1

Thus, 80° pulling optimally balanced carbohydrate allocation and hormone signaling, providing a data-driven benchmark for canopy management in high-density Korla fragrant pear orchards.

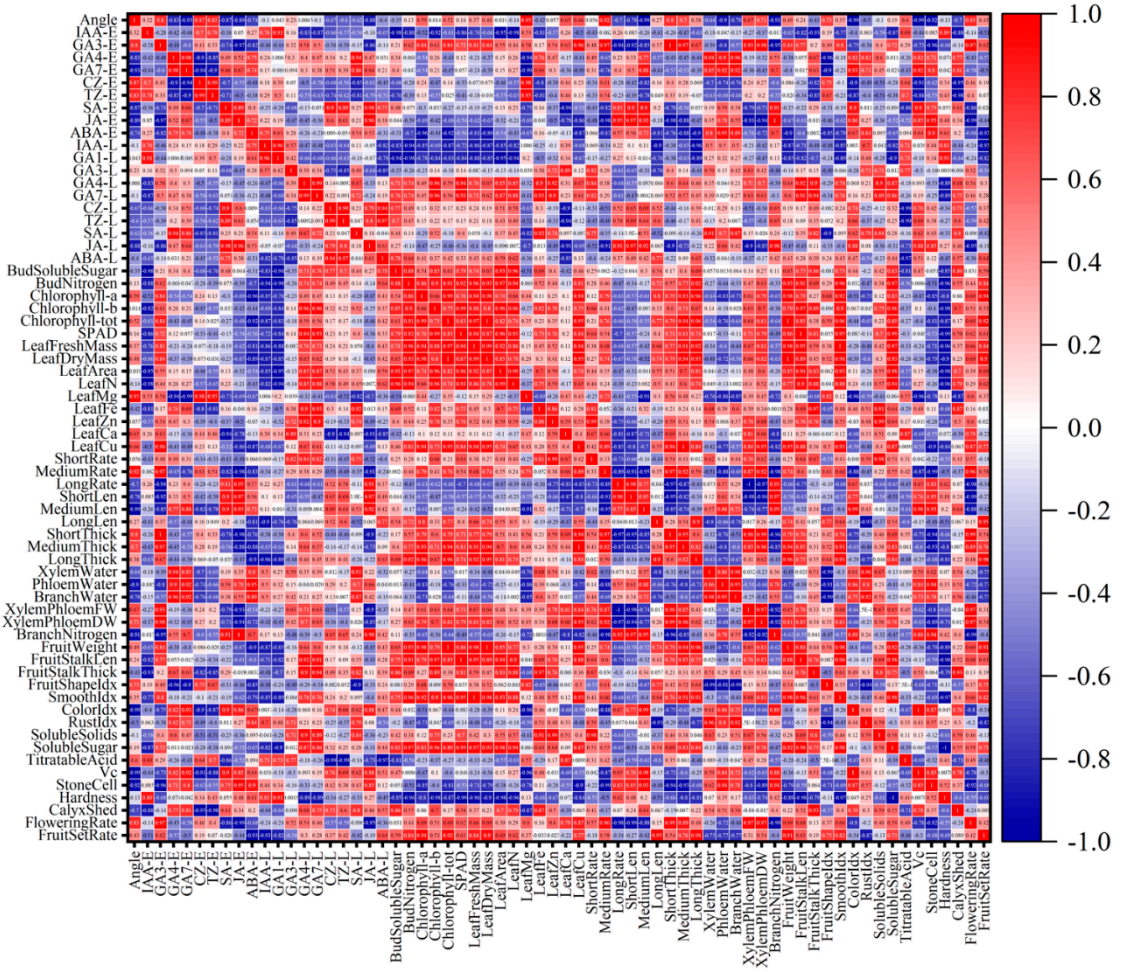

Figure 15. Correlation heatmap among 57 physiological and quality traits of Pyrus sinkiangensis under four branch-bending angles (40°, 60°, 80°, and 100°). Hormone variables are arranged in two blocks, early-phase (left) and late-phase (right), to visualize temporal dynamics. The red–blue gradient indicates positive–negative correlations; color intensity is proportional to Pearson |r|. Abbreviations follow exactly those used in Figures 2–8.

Table 1. Eigenvalues and variance contributions of the three extracted principal components.

Component	Eigenvalue	Variance (%)	Cumulative (%)
PC1	30.77	47.34	47.34
PC2	20.81	32.01	79.35
PC3	13.42	20.64	100

Table 2. Principal component scores (PC1–PC3) for the four branch-bending angles.

Angle	PC1	PC2	PC3
40°	-1.326	0.384	0.587
60°	0.181	0.689	1.32
80°	0.412	-1.486	0.934
100°	0.046	-0.201	0.201

 doi:10.20944/preprints202512.2343.v1

Table 3. Comprehensive evaluation score (D) and ranking of the four angles based on PCA.

Angle	D value	Rank
40°	0.317	3
60°	0.687	2
80°	0.718	1
100°	0.197	4

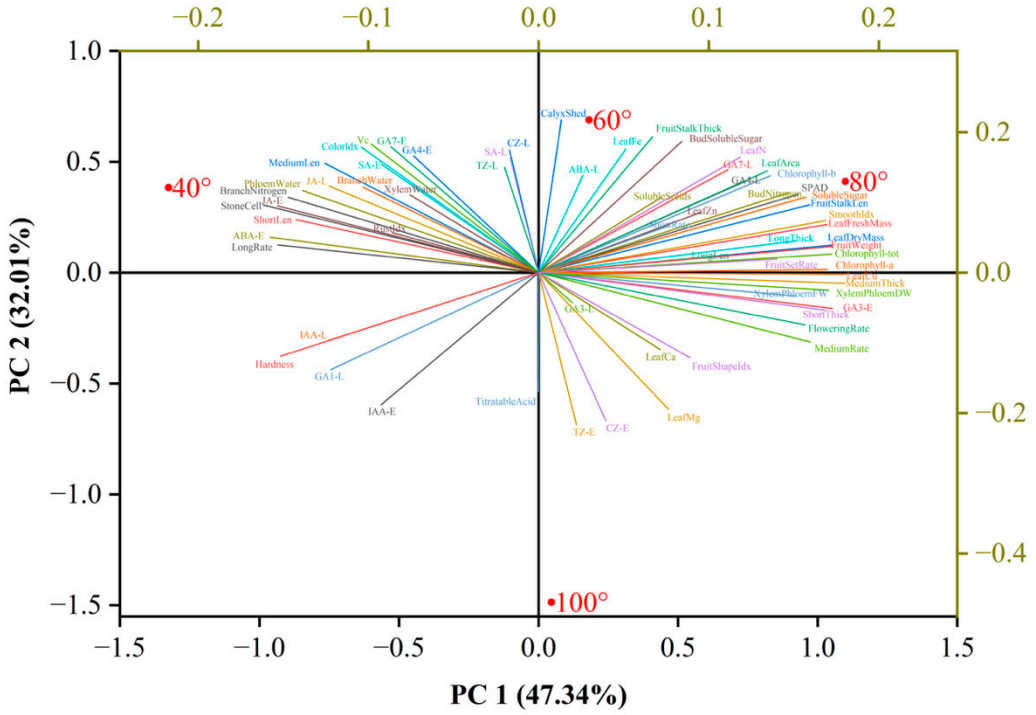

Figure 16. Biplot of principal component analysis (PCA) results for 57 physiological and quality traits of *Pyrus sinkiangensis* at four branch-bending angles (40°, 60°, 80°, and 100°). Sample scores (points) and variable loadings (vectors) are projected onto PC1 and PC2. The 80° treatment is positioned in the positive direction of PC1 and is closely associated with higher soluble sugar, GA_4, GA_7, and fruit set rates. PC1 and PC2 explain 47.34% and 32.01% of the total variance, respectively. Only variables with loadings ≥ |0.5| are displayed.

3. Discussion

To identify the optimal branch bending angle for Korla fragrant pear, we compared four orientations (40°, 60°, 80°, and 100°) and integrated phenological, nutritional, hormonal, leaf- and branch-architecture, and fruit-quality data across the bloom window. The 80° angle consistently outperformed all the treatments, maximizing the fruit set (11.77%) and bud soluble-sugar content (8.84 mg/g DW) and transiently increasing the $GA_{4/7}$ and cytokinin levels, whereas 60° resulted in the highest calyx removal rate (73.33%). Principal component analysis of 57 physiological and quality traits revealed that 80° was the superior compromise between carbon allocation, hormone signaling, and fruit development. We therefore confirm that an 80° bending angle provides a practical benchmark for high-density Korla fragrant pear orchards.

Branch pulling had negligible effects on flowering phenology, with all four angles showing similar 11-day bloom windows (Figure 1). Only the 100° treatment delayed initial flowering by one day and extended petal fall, which is consistent with the view that larger angles can alter vascular flux and phytohormone gradients [20]. However, the conserved flowering duration indicates that the bending angle primarily modulates reproductive intensity rather than developmental timing. The flowering rate increased linearly with increasing bending angle (Figure 2), with the values at 60°, 80°,

 doi:10.20944/preprints202512.2343.v1

and 100°significantly exceeding that at 40°, which aligns with the findings of previous studies on pear flower bud formation [14]. In contrast, fruit set peaked at 80°, not at the maximum angle, revealing an optimal stress window: moderate bending enhances sink strength without imposing excessive mechanical stress that could impair pollen–pistil interactions or ovule longevity [21]. The calyx removal rate reached 73.33% at 60°, which was statistically comparable to that at 80° (71%, $P > 0.05$), indicating that both angles effectively promoted calyx abscission. However, 80° additionally maximized the fruit set and quality, making it the superior integrated solution.

Leaf physiology and source capacity were strongly angle dependent, with 80° pulling producing the greatest leaf area (59.51 cm^2), highest chlorophyll content (3.11 mg/g DW), and elevated leaf nitrogen (23.36 mg/g DW), magnesium (46.43 mg/g DW), and copper (23.64 mg/g DW) concentrations (Figure 3). These results align with those of Lauri et al. [22], who reported that branch orientation in apple significantly affects leaf photosynthesis and fruit quality. Enhanced leaf nitrogen and magnesium under 80° likely improved Rubisco activity and thylakoid electron transport, which is consistent with our previous findings that bending caused increases in chlorophyll and carotene levels. Under these conditions, this treatment changed plant performance from upright to a more dispersed canopy. Sufficient light facilitates optimal photosynthesis in plants, affecting the processes of flowering and fruit formation [23]. The concomitant increase in leaf copper concentration may support plastocyanin function in the photosynthetic electron chain, further affecting the growth rate and photosynthetic parameters [24]. This "larger-greener-richer" leaf phenotype at 80° directly contributed to the elevated bud soluble-sugar content observed at this angle, creating a strong carbon foundation for floral induction.

Branch architecture and water–nitrogen partitioning were also optimized at 80° (Figures 4 and 5). The percentage of medium fruiting spurs (5–15 cm) peaked at 80° (41.1%), whereas long spurs (>15 cm) were suppressed from 59.6% at 40° to ~40% at 60–100°. This reallocation toward compact, efficient fruiting units improves assimilate unloading to reproductive sinks and reduces vegetative–reproductive growth competition [25]. Although total branch nitrogen was highest at 40° (29.4 mg/g DW), the xylem-to-phloem dry-weight ratio peaked at 80° (1.78), indicating a more balanced hydraulic architecture that limits lignin deposition while maintaining sugar-transport capacity [26]. The reduced total branch water content at 80° (56.2%) likely reflects adjustments in the xylem anatomy, a common acclimation to moderate bending stress that reduces the resistance of water transport and buffers xylem pressure. This enhances drought tolerance in arid-region orchards [27]. These branch-level adjustments underpin the superior reproductive performance at 80° by concentrating resources in phloem pathways while minimizing hydraulic overload.

Bud nutrient status confirmed the C/N theory of floral induction (Figure 6). Compared with nitrogen, moderate pulling (60–80°) increased bud carbon accumulation; the relatively high C/N ratio strongly promoted flower-bud differentiation [28]. These findings are congruent with those of Wene Zhang et al. [29], who demonstrated that carbohydrate status interacts with nitrogen signaling to regulate floral commitment in deciduous fruit trees. The higher bud nitrogen at 80° (16.59 mg/g DW) likely supported protein synthesis for floral meristem identity genes, as reported in the Journal of Integrative Agriculture, where GA signaling integrates nitrogen status to activate floral integrators [30]. Thus, the 80° angle synchronizes carbon surplus with adequate nitrogen, creating a metabolic state optimal for floral commitment.

Hormonal dynamics revealed a temporally precise signaling cascade unique to 80° (Figures 7–11). The transient increase in the $GA_4/_7$ ratio on 28 April (50.6 and 1.34 ng/g DW) synchronized with the increase in the ABA concentration (2,058 ng/g DW), resulting in the formation of a "GA–ABA switch" that triggered ovary growth while preventing calyx persistence [31]. Critically, the IAA concentration at 80° followed a "flat–surge–plateau" trajectory: it remained low during calyx abscission (≤1.2 ng/g DW) but then increased steadily to 2.05 ng/g DW by 4 May, after which it stabilized at levels significantly higher than those at all other angles. This late-plateau IAA pattern at 80° likely reinforced ovary sink strength and antagonized ABA-induced fruit drop, directly underpinning the 11.77% fruit set rate. Cytokinin dynamics further supported this model: zeatin

 doi:10.20944/preprints202512.2343.v1

remained low (≤0.15 ng/g DW) during calyx abscission to avoid reactivating cell division and then increased to 0.27–0.29 ng/g DW on 4 May—levels sufficient to promote ovary development but below the threshold that would risk persistent calyx formation [32].

Fruit quality traits were comprehensively enhanced at 80° (Figures 12–14). The 80° treatment produced the heaviest fruit (110.7 g), highest soluble-sugar content (10.08 mg/g DW), and optimal sugar/acid ratio (17.08) while maintaining a low stone-cell content (0.49 mg/g DW). Increased fruit weight under 80° pulling reflects a stronger assimilate supply during the cell division and expansion phases, as demonstrated in pear, where optimal branch angles promote fruit development through enhanced phloem loading [33]. The reduced stone-cell content under 80° likely results from coordinated $GA_4/_7$ and IAA signaling that regulates lignin deposition in sclereids. Low concentrations of IAA can reduce lignification and stone cell formation in pear flesh, whereas high concentrations promote these processes, demonstrating the concentration-dependent nature of auxin regulation; gibberellin can inhibit stone cell formation and lignin deposition in 'Nanguo' pear, with the mechanism being related to the downregulation of PuPRX73 and its upstream activating factor expression [34,35]. Although 60° and 80° resulted in comparable calyx removal rates, 80° additionally maximized the fruit set and quality, providing a clear market advantage.

Pixel-level dissection of the correlation heatmap revealed a system-wide pattern: a bell-shaped warm domain centered at 60–80° that spanned hormones, carbon, leaf economics, spur architecture, branch hydraulics, stone cells, and fruit set (Figure 15). This visual synthesis confirms that 80° is not merely a local optimum but a system-wide attractor that synchronizes multiple physiological modules, which is consistent with the view that the branch angle is a key driving factor for the photosynthetic performance and outcomes of apple leaves [36].

The PCA biplot corroborates this system-level interpretation (Figure 16). PC1 (47.34% variance) segregated 80° (score = 0.412) from 100° (0.046) along the vectors of soluble sugars, $GA_4/_7$, and fruit weight, quantifying the carbon–hormone synergy. PC2 (32.01%) captured ABA-SA antagonism, with 80° positioned negatively (-1.486), indicating suppressed stress signaling despite mechanical bending. The clustering of quality traits (sugar/acid ratio, stone cells) with 80° on PC1 confirms its economic superiority, while 100° aligned with titratable acid, suggesting that overbending may divert carbon to malic acid biosynthesis. This multivariate perspective avoids single-trait bias and establishes 80° as a data-driven canopy management target.

While this study was conducted in a single orchard and season, the results provide testable hypotheses for multiyear, multilocation trials that are currently underway. The 15-day hormone monitoring window precisely targeted the critical bloom period, and future work will extend to the prebudbreak and fruit development phases to construct a complete temporal hormone profile. The specificity of the 'Dangshansuli'/'Zhongai No. 1' rootstock/scion combination is being evaluated through parallel trials on alternative rootstocks. To establish causality, decapitation and girdling experiments are in progress to directly test the sugar–flow–hormone–transport hierarchy, with preliminary results supporting a carbon-driven GA_4 synthesis hypothesis.

In conclusion, this study demonstrated that an 80° bending angle synchronizes carbohydrate supply, hormone signaling, and fruit quality in Korla fragrant pear, providing a low-cost, nonchemical tool for precision canopy management. The sugar–hormone module identified here offers a mechanistic framework for other rosaceous species in which floral induction limits yield. Future integration of real-time hormone profiling with machine learning may enable dynamic, climate-adaptive branch management strategies for next-generation high-density orchards.

4. Conclusions

In this study, 57 physiological and quality traits were integrated to identify the optimal branch bending angle for high-density cultivation of Korla fragrant pear. An **80° angle** emerged as the superior solution, systemically restructuring the "source–sink–signal" cascade. First, the leaf photosynthetic capacity significantly increased, with the leaf area expanding to 59.51 cm^2 and the chlorophyll content increasing by 30%. This was followed by the optimization of branch transport

 doi:10.20944/preprints202512.2343.v1

architecture, where the percentage of medium fruiting spurs reached 41.1%, and a "dry yet functional" hydraulic framework was established (xylem:phloem dry weight ratio = 1.78), ensuring efficient sugar transport to buds. Ultimately, the bud soluble sugar content peaked (8.84 mg/g DW), triggering a precise hormonal regulatory module—a transient GA_4/GA_7 surge on 28 April coordinated with ABA to promote calyx abscission, followed by a sustained IAA plateau (2.05 ng/g DW) and cytokinin (0.27–0.29 ng/g DW), synergistically enhancing ovary development. This cascade maximized the fruit set (11.77%), yielding a single weight of 110.7 g, a sugar/acid ratio of 17.08, and a reduced stone cell content to 0.49 mg/g DW, indicating that the optimal comprehensive quality was achieved.

Supplementary Materials: The following supporting information can be downloaded at the website of this paper posted on Preprints.org.

Acknowledgments: This work was supported by the National Science and Technology Support Program of China: "Effects of Branch Spreading Angles on the Growth and Fruit-Bearing of Young 'Korla Fragrant Pear' Trees with 'Zhongdai No. 1' as the Dwarf Interstem" (Grant No. xjnk-2021014). The authors thank Turpan Experimental Station, Xinjiang Academy of Agricultural Sciences, for technical support; the College of Horticulture, Xinjiang Agricultural University, for providing experimental instruments and laboratory facilities; and the staff of Sciences Fruit and Vegetable Research Institute of Xinjiang Uygur Autonomous Region Academy of Agricultural Sciences (National Fruit Tree Germplasm Resources Luntai Fruit Tree Resource Garden) for technical assistance and orchard maintenance. The corresponding author (Mansur Nasir) is especially grateful to his wife, Zulayat Yusup, and their daughter, Marfina Mansur, who just turned three months old, for their unwavering love and support throughout this research.

Conflicts of interest: The authors declare that they have no known competing financial interests or personal relationships that could have appeared to influence the work reported in this paper.

Abbreviations

ABA, abscisic acid; C/N, Carbon/Nitrogen ratio; $CI_1/CI_2/CI_3$, Comprehensive Index 1/2/3; CZ, cis-zeatin; D, Comprehensive Evaluation Score; DW, dry weight; E/L, Early-/Late-phase; GA, gibberellin; $GA_1/GA_3/GA_4/GA_7$, gibberellin $A_1/A_3/A_4/A_7$; IAA, indole-3-acetic acid; ICP–OES, inductively coupled plasma optical emission spectrometry; JA, jasmonic acid; LC-MS/MS, liquid chromatography-tandem mass spectrometry; *M. domestica*, *Malus domestica*; PC1/PC2/PC3, Principal Component 1/2/3; PCA, principal component analysis; *P. communis*, *Pyrus communis* L.; *P. persica*, *Prunus persica* (L.) Batsch; *P. sinkiangensis*, *Pyrus sinkiangensis* Yü; PIabs, Performance Index on absorption basis; PSII, photosystem II; QA, primary quinone electron acceptor of PSII; QB, secondary quinone electron acceptor of PSII; RC, reaction center; REo/RC, electron flux reducing end electron acceptors per RC; ROS, reactive oxygen species; SA, salicylic acid; SE, standard error; SPAD, Soil Plant Analyzer Development; *S. samarangense*, *Syzygium samarangense*; TZ, trans-zeatin.

References

1. Han, M.; Li, B.; Zhang, L.; Wang, Y.; Han, Z. Effects of shoot bending on lateral branch formation and hydraulics in apple. *J. Exp. Bot.* **2007**, *58*, 3537–3547. DOI: 10.1093/jxb/erm197.
2. Zhang, Y.; et al. A core regulatory pathway controlling rice tiller angle mediated by LAZY1-dependent asymmetric auxin distribution. *Plant Cell* **2018**, *30*, 1461–1475. DOI: 10.1105/tpc.18.00044.
3. Cai, H.; Zhang, W.; Wu, L.; et al. Effects of branch bending angle on leaf nutrition, flower formation and nut quality of Qianhe 7 walnut. *J. Fruit Sci.* **2022**, *39*, 60–67. DOI: 10.13925/j.cnki.gsxb.20210330. (In Chinese with English abstract)
4. Zhang, B.; Zheng, F.; Geng, W.; Du, H.; Xiao, Y.; Peng, F. Effect of branch bending on the canopy characteristics and growth of peach (*Prunus persica* (L.) Batsch). *Agronomy* **2023**, *13*, 1058. DOI: 10.3390/agronomy13041058.

 doi:10.20944/preprints202512.2343.v1

5. Cui, H.; Ablat, N.; Wang, R.; et al. Effects of branch bending angle on photosynthetic and chlorophyll fluorescence parameters of 'Zhong'ai 1' dwarfing inter-stock Korla fragrant pear. *Xinj. Agric. Sci.* **2022**, *59*, 1–8. DOI: 10.6048/j.issn.1001-4330.2022.11.006. (In Chinese with English abstract)
6. Chen, Y.; Ma, W.; Feng, J.; Li, L. Branching angles in the modulation of plant architecture: Molecular mechanisms, dynamic regulation, and evolution. *Plant Commun.* **2025**, *6*, 101292. DOI: 10.1016/j.xplc.2025.101292.
7. Zhang, M.; Ma, F.; Shu, H.; Han, M. Branch bending affected floral bud development and nutrient accumulation in shoot terminals of 'Fuji' and 'Gala' apples. *Acta Physiol. Plant.* **2017**, *39*, 156. DOI: 10.1007/s11738-017-2450-5.
8. Choi, H.-S.; Ryu, H.-U.; Gu, M.; Jung, S.-K.; Ryu, J.-H. Effect of the timing and duration of downward bending of branches on growth and fruit quality in 'Fuji Mishima' apple trees. *J. Hortic. Sci. Biotechnol.* **2012**, *87*, 305–310. DOI: 10.1080/14620316.2012.11512868.
9. Khandaker, M.M.; Ismail, N.H.; Abdulrahman, M.D.; et al. Effects of branch bending angle on growth and flowering of wax apple (*Syzygium samarangense*). *Plant Arch.* **2020**, *20*, 5907–5913. DOI: 10.51470/PLANTARCHIVES.2020.V20I2.5907.
10. Khandaker, M.M.; Ismail, N.H.; Abdullahi, U.A.; et al. Tree physiology, fruit growth and nutrient elements of wax apple (*Syzygium samarangense*) as affected by branch bending angle. *Basrah J. Agric. Sci.* **2021**, *34*, 206–221. DOI: 10.37077/25200860.2021.34.1.18.
11. Xinjiang Uygur Autonomous Region Forestry and Grassland Administration. Current Status and Prospects of Xinjiang Fruit Industry. Xinjiang Uygur Autonomous Region Forestry and Grassland Administration, 2025. Available online: https://lcj.xinjiang.gov.cn/lcj/c114734/202504/d7f1e6196b9841f38fe91b3e52f4401e.shtml (accessed on 10 November 2025).
12. Nasir, M.; Du, R.Q.; Chen, X.Y.; Zhou, W.Q.; Niu, Y.Y.; Niyaz, A.; Liao, K. Pollination compatibility and pollen xenia of Xinjiang pear cultivars with 'Kuerlexiangli' pear. *J. Fruit Sci.* **2019**, *36*, 447–457. DOI: 10.13925/j.cnki.gsxb.20180453.
13. Colaric, M.; Stampar, F.; Hudina, M. Effects of branch bending on the levels of carbohydrates and phenolic compounds in 'Conference' pear leaves. *J. Hortic. Sci. Biotechnol.* **2007**, *82*, 815–821. DOI:10.1080/14620316.2007.11512311.
14. Colaric, M.; Stampar, F.; Hudina, M. Bending affects phenolic content of William pear leaves. *Acta Agric. Scand. B Soil Plant Sci.* **2007**, *57*, 187–192. DOI: 10.1080/09064710600834350.
15. Colaric, M.; Stampar, F.; Solar, A.; et al. Influence of branch bending on sugar, organic acid and phenolic content in fruits of 'Williams' pears (*Pyrus communis* L.). *J. Sci. Food Agric.* **2006**, *86*, 2463–2467. DOI:10.1002/jsfa.2644
16. Wilson, B.F. Apical control of branch growth and angle in woody plants. *Am. J. Bot.* **2000**, *87*, 601–607. DOI: 10.2307/2656846.
17. Masson, P.; Dalix, T.; Bussière, S. Determination of major and trace elements in plant samples by inductively coupled plasma–mass spectrometry. *Commun. Soil Sci. Plant Anal.* **2010**, *41*, 231–243. DOI: 10.1080/00103620903460757.
18. Millard, P.; Grelet, G.A. Nitrogen storage and remobilization in trees: Ecophysiological relevance in a changing world. *Tree Physiol.* **2010**, *30*, 1083–1095. DOI: 10.1093/treephys/tpq054.
19. Ito, A.; Tuan, P.A.; Saito, T.; et al. Changes in phytohormone content and associated gene expression throughout the stages of pear dormancy. *Tree Physiol.* **2021**, *41*, 529–543. DOI: 10.1093/treephys/tpz101.
20. Larson, P.R.; Richards, J.H. Lateral branch vascularization: Its circularity and its relation to anisophylly. *Can. J. Bot.* **1981**, *59*, 2577–2591. DOI: 10.1139/b81-309.
21. Timerman, D.; Barrett, S.C. The biomechanics of pollen release: New perspectives on the evolution of wind pollination in angiosperms. *Biol. Rev.* **2021**, *96*, 2146–2163. DOI: 10.1111/brv.12745.
22. Hashimoto, T. Studies on the magnesium metabolism of crops (Part 1) The balance among magnesium, calcium and potassium in free and bound forms at the flowering stage of soy-bean plants. *Soil Sci. Plant Nutr.* **1956**, *2*, 123–130. DOI: 10.1080/00380768.1956.10431871.

 doi:10.20944/preprints202512.2343.v1

23. Peng, H.; Kroneck, P.M.; Küpper, H. Toxicity and deficiency of copper in *Elsholtzia splendens* affect photosynthesis biophysics, pigments and metal accumulation. *Environ. Sci. Technol.* **2013**, *47*, 6120–6128. DOI: 10.1021/es3050746.
24. Wünsche, J.N.; Lakso, A.N. The relationship between leaf area and light interception by spur and extension shoot leaves and apple orchard productivity. *HortScience* **2000**, *35*, 1202–1206. DOI: 10.21273/HORTSCI.35.7.1202.
25. Pawar, R.; Rana, V.S. Manipulation of source-sink relationship in pertinence to better fruit quality and yield in fruit crops: A review. *Agric. Rev.* **2019**, *40*, 200–207. DOI: 10.18805/ag.R-1934.
26. Pegler, J.L.; Grof, C.P.; Patrick, J.W. Sugar loading of crop seeds—A partnership of phloem, plasmodesmal and membrane transport. *New Phytol.* **2023**, *239*, 1584–1602. DOI: 10.1111/nph.19058.
27. Klein, T.; Zeppel, M.J.; Anderegg, W.R.; et al. Xylem embolism refilling and resilience against drought-induced mortality in woody plants: Processes and trade-offs. *Ecol. Res.* **2018**, *33*, 839–855. DOI: 10.1007/s11284-018-1588-y.
28. Wan, C.; Mi, L.; Chen, B.; Li, J.; Huo, H.; Xu, J.; Chen, X. Effects of nitrogen during nursery stage on flower bud differentiation and early harvest after transplanting in strawberry. *Braz. J. Bot.* **2018**, *41*, 1–10. DOI: 10.1007/s40415-017-0417-9.
29. Zhang, W.; Li, J.; Zhang, W.; Njie, A.; Pan, X. The changes in C/N, carbohydrate, and amino acid content in leaves during female flower bud differentiation of *Juglans sigillata*. *Acta Physiol. Plant.* **2022**, *44*, 19. DOI: 10.1007/s11738-021-03328-9.
30. Zhang, X.X. Effect of exogenous GA3 on flowering quality, endogenous hormones, and hormone- and flowering-associated gene expression in forcing-cultured tree peony (*Paeonia suffruticosa*). *J. Integr. Agric.* **2019**, *18*, 1295–1311. DOI: 10.1016/S2095-3119(18)62131-8.
31. Shuai, H.; Meng, Y.; Luo, X.; Chen, F.; Zhou, W.; Dai, Y.; Qi, Y.; Du, J.; Yang, F.; Liu, J.; Yang, W. Exogenous auxin represses soybean seed germination through decreasing the gibberellin/abscisic acid (GA/ABA) ratio. *Sci. Rep.* **2017**, *7*, 12620. DOI: 10.1038/s41598-017-13093-w.
32. Ali, S.A.M.; Mohd, C.C.; Latip, J. Comparison of phenolic constituent in *Hibiscus sabdariffa* cv. UKMR-2 calyx at different harvesting times. *Sains Malaysiana* **2019**, *48*, 1417–1424. DOI: 10.17576/jsm-2019-4807-10.
33. Law, T.L.; Lang, G.A. Planting angle and meristem management influence sweet cherry canopy development in the "Upright fruiting offshoots" training system. *HortScience* **2016**, *51*, 1010–1015. DOI: 10.21273/HORTSCI.51.8.1010.
34. Wang, Y.; Wang, Q.; Zhang, F.; Han, C.; Li, W.; Ren, M.; Wang, Y.; Qi, K.; Xie, Z.; Zhang, S.; Tao, S. PbARF19-mediated auxin signaling regulates lignification in pear fruit stone cells. *Plant Sci.* **2024**, *344*, 112103. DOI: 10.1016/j.plantsci.2024.112103.
35. Xu, M.; He, S.; Zhang, H.; Gao, S.; Yin, M.; Li, X.; Du, G. Gibberellin regulates the synthesis of stone cells in 'Nanguo' pear via the PuMYB91-PuERF023 module. *Physiol. Plantarum* **2025**, *177*, e70074. DOI: 10.1111/ppl.70074.
36. Yang, S.; Mao, J.; Zuo, C.; Tian, F.; Li, W.; Dawuda, M.M.; Ma, Z.; Chen, B. Branch age and angle as crucial drivers of leaf photosynthetic performance and fruiting in high-density planting: A study case in spur-type apple "Vallee Spur" (*Malus domestica*). *Sci. Hortic.* **2019**, *246*, 898–906. DOI: 10.1016/j.scienta.2018.11.084.